



Calhoun: The NPS Institutional Archive

DSpace Repository

Theses and Dissertations

1. Thesis and Dissertation Collection, all items

2014-09

Using Cloudat and the A-Train to estimate tropical cyclone intensity in the western North Pacific

Seibold, Jeffrey K.

Monterey, California. Naval Postgraduate School

<http://hdl.handle.net/10945/43997>

This publication is a work of the U.S. Government as defined in Title 17, United States Code, Section 101. Copyright protection is not available for this work in the United States.

Downloaded from NPS Archive: Calhoun



<http://www.nps.edu/library>

Calhoun is the Naval Postgraduate School's public access digital repository for research materials and institutional publications created by the NPS community.

Calhoun is named for Professor of Mathematics Guy K. Calhoun, NPS's first appointed -- and published -- scholarly author.

**Dudley Knox Library / Naval Postgraduate School
411 Dyer Road / 1 University Circle
Monterey, California USA 93943**



**NAVAL
POSTGRADUATE
SCHOOL**

MONTEREY, CALIFORNIA

THESIS

**USING CLOUDSAT AND THE A-TRAIN TO ESTIMATE
TROPICAL CYCLONE INTENSITY IN THE WESTERN
NORTH PACIFIC**

by

Jeffrey K. Seibold

September 2014

Thesis Advisor:
Second Reader:

Patrick A. Harr
Qing Wang

Approved for public release; distribution is unlimited

THIS PAGE INTENTIONALLY LEFT BLANK

REPORT DOCUMENTATION PAGE

Form Approved OMB No. 0704-0188

Public reporting burden for this collection of information is estimated to average 1 hour per response, including the time for reviewing instruction, searching existing data sources, gathering and maintaining the data needed, and completing and reviewing the collection of information. Send comments regarding this burden estimate or any other aspect of this collection of information, including suggestions for reducing this burden, to Washington Headquarters Services, Directorate for Information Operations and Reports, 1215 Jefferson Davis Highway, Suite 1204, Arlington, VA 22202-4302, and to the Office of Management and Budget, Paperwork Reduction Project (0704-0188) Washington DC 20503.

1. AGENCY USE ONLY (Leave blank)	2. REPORT DATE September 2014	3. REPORT TYPE AND DATES COVERED Master's Thesis
4. TITLE AND SUBTITLE USING CLOUDSAT AND THE A-TRAIN TO ESTIMATE TROPICAL CYCLONE INTENSITY IN THE WESTERN NORTH PACIFIC		5. FUNDING NUMBERS
6. AUTHOR(S) Jeffrey K. Seibold		
7. PERFORMING ORGANIZATION NAME(S) AND ADDRESS(ES) Naval Postgraduate School Monterey, CA 93943-5000		8. PERFORMING ORGANIZATION REPORT NUMBER
9. SPONSORING /MONITORING AGENCY NAME(S) AND ADDRESS(ES) N/A		10. SPONSORING/MONITORING AGENCY REPORT NUMBER
11. SUPPLEMENTARY NOTES The views expressed in this thesis are those of the author and do not reflect the official policy or position of the Department of Defense or the U.S. Government. IRB protocol number ____ N/A ____.		
12a. DISTRIBUTION / AVAILABILITY STATEMENT Approved for public release; distribution is unlimited		12b. DISTRIBUTION CODE
13. ABSTRACT (maximum 200 words) CloudSat joined the A-Train constellation in June 2006 to enhance the understanding of the global heat budget by providing measurements of cloud properties on a global scale, and provide the first statistics on the vertical structure of clouds from space. The data collected by CloudSat could provide forecasters a tool in estimating tropical cyclone (TC) intensity in areas where <i>in situ</i> measurements are scarce. This thesis expanded the data set and methodology employed by Luo et al. (2008) to estimate the maximum sustained winds using satellite based cloud-top slope estimates. The method requires an eye or near-eye overpass as well as simultaneous and accurate measurements of cloud-top height, cloud-top temperature, and cloud profiling information across the center of a storm. A primary objective of this thesis was to examine sensitivities of estimated maximum wind to the overpass distance to the TC center, the TC intensity, and TC structure asymmetries due to vertical wind shear. A significant dependency was identified to the distance between the satellite overpass and TC center. In general, there was an over-estimation of weaker storms and an under-estimation of strong storms. The greatest accuracy is found where the satellite overpass was relatively near the TC center.		

14. SUBJECT TERMS CloudSat, A-Train, CloudSat Intensity Forecasting, Moist Static Energy, Cloud-top Height, Cloud-top Temperature, Cloud Profiling Radar, Reflectivity, MODIS		15. NUMBER OF PAGES 71	
16. PRICE CODE			
17. SECURITY CLASSIFICATION OF REPORT Unclassified	18. SECURITY CLASSIFICATION OF THIS PAGE Unclassified	19. SECURITY CLASSIFICATION OF ABSTRACT Unclassified	20. LIMITATION OF ABSTRACT UU

THIS PAGE INTENTIONALLY LEFT BLANK

Approved for public release; distribution is unlimited

**USING CLOUDSAT AND THE A-TRAIN TO ESTIMATE TROPICAL
CYCLONE INTENSITY IN THE WESTERN NORTH PACIFIC**

Jeffrey K. Seibold
Lieutenant, United States Navy
B.S., Purdue University, 2004

Submitted in partial fulfillment of the
requirements for the degree of

**MASTER OF SCIENCE IN METEOROLOGY AND PHYSICAL
OCEANOGRAPHY**

from the

NAVAL POSTGRADUATE SCHOOL
September 2014

Author: Jeffrey K. Seibold

Approved by: Patrick A. Harr, Ph.D.
Thesis Advisor

Qing Wang, Ph.D.
Second Reader

Wendell A. Nuss, Ph.D.
Chair, Department of Meteorology

THIS PAGE INTENTIONALLY LEFT BLANK

ABSTRACT

CloudSat joined the A-Train constellation in June 2006 to enhance the understanding of the global heat budget by providing measurements of cloud properties on a global scale, and provide the first statistics on the vertical structure of clouds from space. The data collected by CloudSat could provide forecasters a tool in estimating tropical cyclone (TC) intensity in areas where *in situ* measurements are scarce.

This thesis uses data obtained from CloudSat and the A-Train to estimate the maximum sustained winds in TCs from 2006-2013 using satellite based cloud-top slope estimates. The method requires an eye or near-eye overpass as well as simultaneous and accurate measurements of cloud-top height, cloud-top temperature, and cloud profiling information across the center of a storm.

A primary objective of this thesis was to examine sensitivities of estimated maximum wind to the overpass distance to the TC center, the TC intensity, and TC structure asymmetries due to vertical wind shear. A significant dependency was identified to the distance between the satellite overpass and TC center. In general, there was an over-estimation of weaker storms and an under-estimation of strong storms. The greatest accuracy is found where the satellite overpass was relatively near the TC center.

THIS PAGE INTENTIONALLY LEFT BLANK

TABLE OF CONTENTS

I.	INTRODUCTION.....	1
A.	MOTIVATION	1
B.	OBJECTIVE	2
II.	BACKGROUND	5
A.	CLOUDSAT CONCEPT.....	5
B.	CLOUDSAT MISSION AND DATA FLOW.....	7
C.	CLOUD PROFILING RADAR.....	9
D.	ESTIMATING TROPICAL CYCLONE INTENSITY	10
III.	METHODOLOGY	17
A.	DATA	17
1.	Data Source.....	17
2.	Data Format	21
3.	CloudSat Products	22
a.	2B- <i>GEOPROF</i>	23
b.	<i>MODIS-AUX</i>	24
4.	CloudSat Fields	24
5.	Measuring Δh^*	27
IV.	ANALYSIS AND RESULTS	29
A.	ANALYSIS	29
B.	COMPARISON AGAINST BEST TRACK DATA.....	30
C.	RESULTS BY CATEGORY.....	32
1.	Saffir-Simpson Scale of Intensity	32
2.	Overpass Distance to TC center	35
3.	Change in Total Moist Static Energy	36
4.	Shear.....	37
V.	CASE STUDIES.....	39
A.	WEAK CORRELATION.....	39
1.	TD BILLIS – 8 July 2006	39
2.	Category 4 CHOI-WAN—15 September 2009.....	40
3.	Category 5 YAGI—21 September 2006.....	41
B.	STRONG CORRELATION	42
1.	Category 1 PRAPIROON—02 August 2006	42
2.	Category 3 NIDA—30 November 2009.....	43
3.	Category 4 KAJIKI—21 October 2007.....	44
VI.	CONCLUSIONS	47
A.	UTILITY OF CPR MEASUREMENTS AND THE A-TRAIN	47
B.	RECOMMENDATIONS.....	48
LIST OF REFERENCES		51
INITIAL DISTRIBUTION LIST		53

THIS PAGE INTENTIONALLY LEFT BLANK

LIST OF FIGURES

Figure 1.	The structure of the A-Train constellation. (from CloudSat Mission 2014).....	5
Figure 2.	CloudSat System Data Flow (from Cooperative Institute for Research in the Atmosphere 2008).....	8
Figure 3.	The energy cycle of a mature TC (from Emanuel 2005).....	13
Figure 4.	Estimated versus best track “observed” tropical storm intensity. Triangles define cases in which CloudSat data were used and circles define cases in which Δh^* was calculated explicitly (from Luo et al. 2008b).....	14
Figure 5.	NRL produced overlay of CHOI-WAN from 15 SEP 2009. The upper panel is an infrared image at 0351 UTC and the lower image is a radar cross section taken along the red line in the upper panel. (from Colorado State University 2014)	17
Figure 6.	Typhoon Ewinar: (from top to bottom) 11- μ m brightness temperature (in kelvins), cloud-top height (in meters), calculated moist static energy (in Kelvin), and CloudSat reflectivity (in decibels referenced to zero) (after Luo et al. 2008b).....	27
Figure 7.	Typhoon Choi-Wan (from top to bottom) cloud-top height (in km), max reflectivity (in dBZ), height of max reflectivity (in km), and CloudSat reflectivity (in dBZ).....	28
Figure 8.	Estimated versus best track tropical cyclone maximum wind speed ($m s^{-1}$) categorized by the Saffir-Simpson intensity scale for all TCs on the left and TCs with a clear center on the right	34
Figure 9.	Estimated versus best track tropical cyclone maximum wind speed ($m s^{-1}$) categorized by the satellite overpass distance to the storm center (in km). All TCs are on the left and only TCs with a clear center are on the right	35
Figure 10.	Estimated versus best track tropical cyclone maximum wind speed ($m s^{-1}$) categorized by the change in total moist static energy from the inner to outer core. All TCs are on the left and only TCs with a clear center are on the right	37
Figure 11.	Estimated versus best track tropical cyclone intensity categorized by storm shear	38
Figure 12.	(a) The 89 GHz Aqua microwave and MTSAT infrared image composite of TD Billis at 1530 UTC 8 July 2006, (b) CloudSat derived cloud-top height (km), (c) maximum reflectivity (dBZ), (d) height of maximum reflectivity (km), (e) reflectivity cross-section (dBZ).....	40
Figure 13.	(a) Infrared image from Aqua at 0351 UTC 15 September 2009 of category four Choi-Wan, (b) Cloud-top height (km), (c) maximum reflectivity (dBZ), (d) height of maximum reflectivity (km), and (e) reflectivity cross-section (dBZ)	41
Figure 14.	(a) Infrared image from Aqua at 1611 UTC 21 September 2006 of category five Yagi, (b) Cloud-top height (km), (c) maximum reflectivity (dBZ), (d) height of maximum reflectivity (km), and (e) reflectivity cross-section (dBZ)	42

Figure 15.	(a) Infrared image from Aqua at 0552 UTC 02 August 2006 of category one Prapiroon, (b) Cloud-top height (km), (c) maximum reflectivity (dBZ), (d) height of maximum reflectivity (km), and (e) reflectivity cross-section (dBZ)	43
Figure 16.	(a) Infrared image from MTSAT at 0430 UTC 30 November 2009 of category four Nida, (b) Cloud-top height (km), (c) maximum reflectivity (dBZ), (d) height of maximum reflectivity (km), and (e) reflectivity cross-section (dBZ)	44
Figure 17.	(a) A 89 GHz Aqua microwave and GMS-6 visible image composite of category five Kajiki at 0330 UTC 21 October 2007, (b) CloudSat derived cloud-top height (km), (c) maximum reflectivity (dBZ), (d) height of maximum reflectivity (km), (e) reflectivity cross-section (dBZ)	45

LIST OF TABLES

Table 1.	Sensor complement and related products of the A-Train. (after Stephens et al. 2002)	7
Table 2.	CPR System characteristics	9
Table 3.	CloudSat TC Overpasses by Distance from 2006–2013.....	18
Table 4.	CloudSat TC statistics by year.....	19
Table 5.	CloudSat TC statistics from 2006-2013 based on Saffir-Simpson scale	19
Table 6.	CloudSat TC Overpasses arranged by Minimum Distance.	20
Table 7.	List of CloudSat level-1 and level-2 products (after Stephens et al. 2002)	23
Table 8.	Listing of geolocation fields within a characteristic HDF File.....	24
Table 9.	Listing of data fields within a characteristic HDF file. Bold entries were used in this study.....	25
Table 10.	CloudSat TC statistics from 2006-2013 of cases containing a clear center stratified by Saffir-Simpson scale.....	30
Table 11.	Intensity prediction based on CloudSat and A-Train measurements.....	31
Table 12.	Average intensity difference ($m s^{-1}$) by Saffir-Simpson scale for all 65 cases	33
Table 13.	Average intensity difference ($m s^{-1}$) by Saffir-Simpson scale for the 22 clear center cases.....	33
Table 14.	Linear correlation between the estimated and actual maximum wind speeds for the TC cases with a clear center. Correlations that are statistically significant at a 95% level are in bold.....	34
Table 15.	As in Table 13, except for distance between the satellite overpass and the storm center.....	36

THIS PAGE INTENTIONALLY LEFT BLANK

LIST OF ACRONYMS AND ABBREVIATIONS

AFSCN	Air Force Satellite Communications Network
AOR	area of responsibility
CALIPSO	cloud-aerosol lidar and infrared pathfinder satellite observations
CIRA	Cooperative Institute for Research in the Atmosphere
CPHC	Central Pacific Hurricane Center
CPR	cloud profiling radar
DOD	Department of Defense
DPC	Data Processing Center
ECMWF	European Centre for Medium-Range Weather Forecasts
EOS	Earth observing system
EOSDIS	Earth observing system data and information system
ESSP	Earth sciences systems pathfinder
HDF	hierarchical data format
MODIS	moderate resolution imaging spectroradiometer
MSE	moist static energy
MSW	maximum sustained winds
NASA	National Aeronautics and Space Administration
NRL	Naval Research Laboratory
PARASOL	polarization and anisotropy of reflectances for atmospheric sciences coupled with observations from lidar
PI	principal investigator
PR	precipitation radar
POLDER	polarization and directionality of the Earth's reflectances
RDT&E SC	research, developmental test and evaluation support center
TC	tropical cyclone
TRMM	tropical rainfall measuring mission
USAF	United States Air Force
WE2007	Wong and Emanuel 2007
WPAC	western North Pacific

THIS PAGE INTENTIONALLY LEFT BLANK

ACKNOWLEDGMENTS

Thank you to my wife, Heather, for her love, encouragement, and support throughout the thesis process. There were many lost nights and weekends together, and I am thankful for her flexibility and understanding nature.

I would also like to thank my thesis advisor, Dr. Pat Harr, for his instruction as both a classroom professor and an advisor. His ability to break down complex concepts is a truly extraordinary trait. I could not have imagined a better mentor and advisor. Many thanks go to all the professors and support staff at NPS for their dedication, expertise and instruction throughout my master's education coursework.

Additionally, I would like to acknowledge Ms. Natalie Tourville, a research associate with CIRA Colorado State University, for her exceptional reachback support. She was always quick to answer any question regarding the CloudSat database.

Finally, to all of my classmates, for their teamwork and camaraderie during our shared NPS journey: I look forward to working with you in future endeavors.

THIS PAGE INTENTIONALLY LEFT BLANK

I. INTRODUCTION

A. MOTIVATION

Satellite technology has revolutionized the way in which we observe the weather, especially over data-sparse oceanic regions where tropical cyclones (TC) occur. Prior to 1960, the year of the first successful weather satellite images, any warning of an approaching TC came from stations located upstream of the TC location. Following the infusion of satellites, facilities such as the National Hurricane Center (NHC), the Joint Typhoon Warning Center (JTWC), and the Central Pacific Hurricane Center (CPHC) utilized real-time images of TCs to aid in their forecasting of the projected path and intensity of these severe storms. These three operational United States (U.S.) agencies are responsible for the tracking and warning of nearly all TC activity worldwide. The JTWC is a U.S. Department of Defense (DOD) agency responsible for issuing TC warnings for the Pacific and Indian Oceans. The NHC located in Miami, FL, is a component of the National Center for Environmental Prediction (NCEP). Its mission is to save lives, mitigate property loss, and improve economic efficiency by issuing the best watches, warnings, forecasts, and analyses of hazardous tropical weather. The Hurricane Specialist Unit (HSU) within the NHC maintains a continuous watch, and provides analyses and forecasts for the North Atlantic and eastern North Pacific basins (National Hurricane Center, 2013). The CPHC issues tropical cyclone products for the central North Pacific from 140 degrees west longitude to the international dateline (Central Pacific Hurricane Center, 2012).

Critical to the ability of these agencies to properly forecast TC activity is accurate and timely measurements of the environment. Over the tropical North Atlantic, aircraft from the United States Air Force (USAF) Reserve and National Oceanic and Atmospheric Administration (NOAA) provide *in situ* measurements of the TC and its environment. Additionally, remotely-sensed data from operational polar-orbiting and geostationary satellites are used to monitor the storm and environment. Over the tropical eastern North Pacific, USAF Reserve aircraft measure the TC and environment whenever

a storm threatens Hawaii. Otherwise, satellite data provide observation of the TC environment.

Since 1987, when aircraft reconnaissance was discontinued in the western North Pacific (WPAC), only satellite data have been available to provide measurements of the TC environment. This is a major disadvantage for JTWC forecasters because the WPAC is the area of the world with the longest TC season and one of the largest geographic forecast regions. Of further and perhaps most significant interest to JTWC forecasters is the impact their forecast accuracy has on naval assets at sea and ashore.

As a DOD agency, JTWC is the principal advisor to military assets such as ships, airfields, and bases throughout their area of responsibility (AOR). The center's accuracy directly influences commanders' decisions on whether to sortie a fleet, airfield, or divert war ships, which consequentially affect the lives of American military members and their families. The cost to sortie a fleet can be astronomical, varying in the neighborhood of tens of millions of dollars (Dorsey, 2003). The decision to sortie is recommended by the Fleet Oceanographer, with the ultimate decision resting with the Fleet Commander. The Fleet Oceanographer bases his or her recommendation on the extent of the 50 kt sustained wind speed probability, which is the maritime destructive threshold. The accuracy of forecasts directly influences the decision-making process and, therefore, the potential to save money when sorties could be avoided.

B. OBJECTIVE

Accurate and near real-time measurements, largely from satellite and ground-based radar installations, have increased the understanding of global weather. By harnessing the abilities of these two technologies in a space environment, a tropical cyclone can be better studied and identified in regions of the globe such as the WPAC, where *in situ* measurements are not available. In April 2006, a new satellite named CloudSat was launched from Vandenberg Air Force Base with the purpose of fusing these two technologies (Stephens et al., 2002). CloudSat became one member of the Afternoon constellation, or A-Train, whose members provide active and passive atmospheric measurements at microwave, infrared, and optical wavelengths. Since TCs

develop over warm ocean waters where *in situ* measurements are scarce, remote sensing capability such as those available via the A-Train are superb tools for observing and monitoring the temporal and spatial evolution of TCs (Mitrescu et al., 2008).

The objective of this thesis is to expand upon the work performed by Luo et al. (2008b), who used methods developed by Wong and Emanuel (2007) to estimate TC intensity via simultaneous and accurate measurements of cloud-top height, cloud-top temperature, and cloud profiling information across the center of a given storm. Their method, hereafter [WE2007], utilizes the model of TCs developed by Emanuel (1986), in which a TC is approximated in a non-hydrostatic and axisymmetric framework. Luo et al. (2008b) used cloud-top temperature provided by MODIS and the cloud-top height and profiling information provided by CloudSat to estimate TC intensity. The computed intensity was then compared remotely to best-track archived data.

Since the Luo et al. study was published in early 2008, it only included TCs from 2006 and 2007. This study will expand their work to include TCs over the WPAC from 2006–2013.

Background material is provided in Chapter II. The data and methodology are described in Chapter III. The analysis and results are presented in Chapter IV. Case studies are presented in Chapter V. Conclusions with future recommendations are outlined in Chapter VI.

THIS PAGE INTENTIONALLY LEFT BLANK

II. BACKGROUND

A. CLOUDSAT CONCEPT

The CloudSat mission, which is designed to enhance the understanding of the global heat budget by measuring cloud properties on a global scale, has provided scientists the ability to analyze tropical cyclones in an unprecedented manner. Direct measurements of the vertical structure of clouds have, until now, been limited to a few ground-based radar sites (Stephens et al., 2002). CloudSat was developed as part of a NASA Earth Sciences Systems Pathfinder (ESSP) mission, which required that the system be built, tested, and launched in a relatively short time interval. The purpose of the CloudSat mission is to measure the vertical structure of clouds from space and simultaneously observe cloud and precipitation. The CloudSat satellite flies as part of a constellation of satellites known as the A-Train (Figure 1).

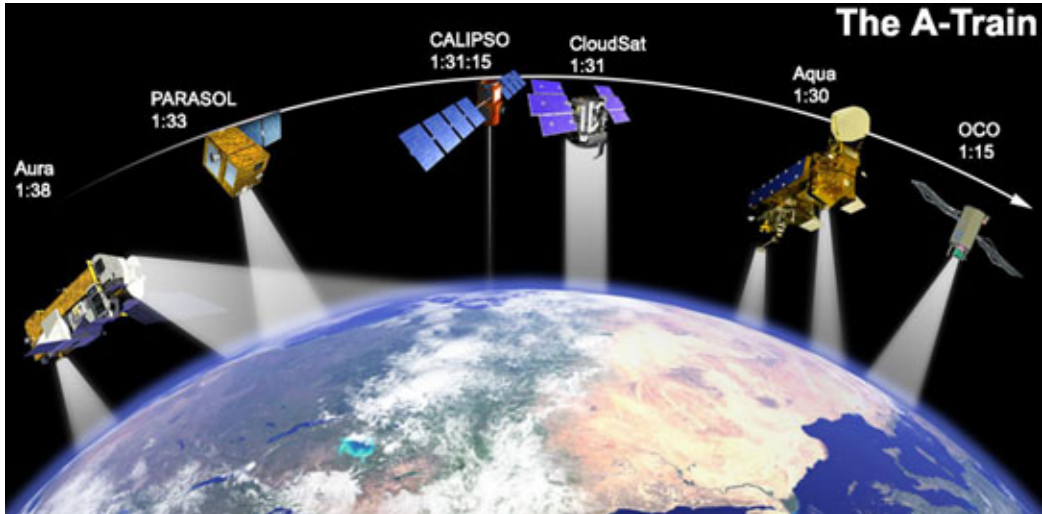


Figure 1. The structure of the A-Train constellation. (from CloudSat Mission 2014)

The A-Train constellation is led by the EOS *Aqua* supporting MODIS and AMSR-E payloads, followed by CloudSat carrying the 94-GHz cloud profiling radar (CPR), then CALIPSO an aerosol lidar detector, followed by PARASOL carrying the POLDER polarimeter, and lastly *Aura* providing microwave high resolution spectral

imaging. Additional details of each member of the A-Train constellation can be found in Table 1. CloudSat is the burdened spacecraft in the A-Train constellation maintaining a formation with *Aqua* and CALIPSO to overlay radar footprints with the lidar footprints of CALIPSO at least 50% of the time. Additionally, the radar footprints fall within the central few kilometers of the *Aqua* MODIS swath (Stephens et al., 2002). Overall the string of satellite stretches across 3000 km in space with each traveling about 7 km sec^{-1} resulting in approximately eight minutes elapsing between the pass of the first to the last satellite of the constellation over any given spot (CloudSat Mission, 2014).

Table 1. Sensor complement and related products of the A-Train.
(after Stephens et al. 2002)

Spacecraft	Payload	Characteristics	Cloud and aerosol products
Aqua Lead constellation spacecraft	MODIS	36-channel visible radiometer, 2300-km-wide swath, variable resolution from 0.25 to 1 km.	Land, ocean, and atmospheric products. The latter include cloud and aerosol optical depths and particle size information, as well as cloud emissivity and cloud-top height.
	AIRS/ AMSU-A/ HSB	Combination of IR and microwave sounders. Swath of $\pm 50^\circ$, resolution of IR sounder ~ 10 km.	Temperature and moisture profiles in clear atmosphere. Some cloud properties.
	AMSR-E	6-channel microwave radiometer. 1445-km swath, asymmetric FOV with variable resolution from $\sim 6 \times 4$ km (89 GHz) to 43×75 km (6 GHz).	LWP, column water vapor, liquid precipitation, principally confined to ocean regions.
	CERES	Broadband and spectral radiances converted to fluxes, resolutions at nadir ~ 20 km.	TOA radiation budget. Primary product is time mean fluxes but instantaneous fluxes are also produced.
CloudSat Lags Aqua by a variable amount but less than 120 s	94-GHz radar (CPR)	500-m vertical range gates from surface to 30 km. High sensitivity. FOV approximately 1.4 km.	Cloud profile information, liquid and ice water content profiles, precipitation. The information is obtained by combining the radar measurements with Aqua measurements including MODIS and AMSR-E as well as with the CALIPSO lidar.
CALIPSO Separation is maintained by CloudSat. Lags CloudSat by 15 ± 2.5 s	Lidar (CALIOP)	532- and 1064-nm channels with depolarization. FOV of approximately 300- and 70-m resolution.	Cloud profile information primarily of upper-tropospheric clouds. Optical depth of thin cirrus. Aerosol profiles with attached optical depth estimates. Aerosol information requires averaging over 10s of kms especially in daylight.
	IIR	3-channel IR radiometer with a FOV of 1 km, swath 64 km.	Cirrus cloud optical properties.
PARASOL Lags CALIPSO by ~ 2 min	POLDER	9-channel polarimeter with channels in the visible and near- infrared. Resolution of 5 m, swath of 400 km.	Cloud and fine mode aerosol optical depths and particle sizes.
Aura Lags Aqua by about 15 min	HIRDLS	IR limb sounder.	Trace gases and stratospheric aerosol.
	MLS	Microwave limb sounder.	Trace gases, ice content of thin upper- tropospheric cloud.
	TES	IR imaging spectrometer, 0.5×5 km resolution, narrow swath and variable pointing.	Trace gases, could also provide high spectral resolution data on clouds.
	OMI	UV grating spectrometer, 13×24 km resolution.	Ozone and aerosol index.

B. CLOUDSAT MISSION AND DATA FLOW

The CloudSat mission is a joint effort by Colorado State University, several NASA entities, the ECMWF, the Air Force, and additional national and international

organizations. It was launched in April 2006 from Vandenberg Air Force Base on a Delta II rocket, and then was assembled into the A-Train formation in June of 2006. CloudSat achieved several firsts upon its activation including statistics on the vertical structure of clouds, global estimates of the percentage of clouds that produce rain, vertically resolved estimates of how much water and ice are in clouds, ability to detect snowfall from space, estimates of how efficiently the atmosphere produces rain from condensates, and first observationally-based estimate of how much clouds contribute to the vertical distribution of atmospheric heating (Jet Propulsion Laboratory, 2005). The large number of agencies working on the project creates a complex data flow, as outlined in Figure 2.

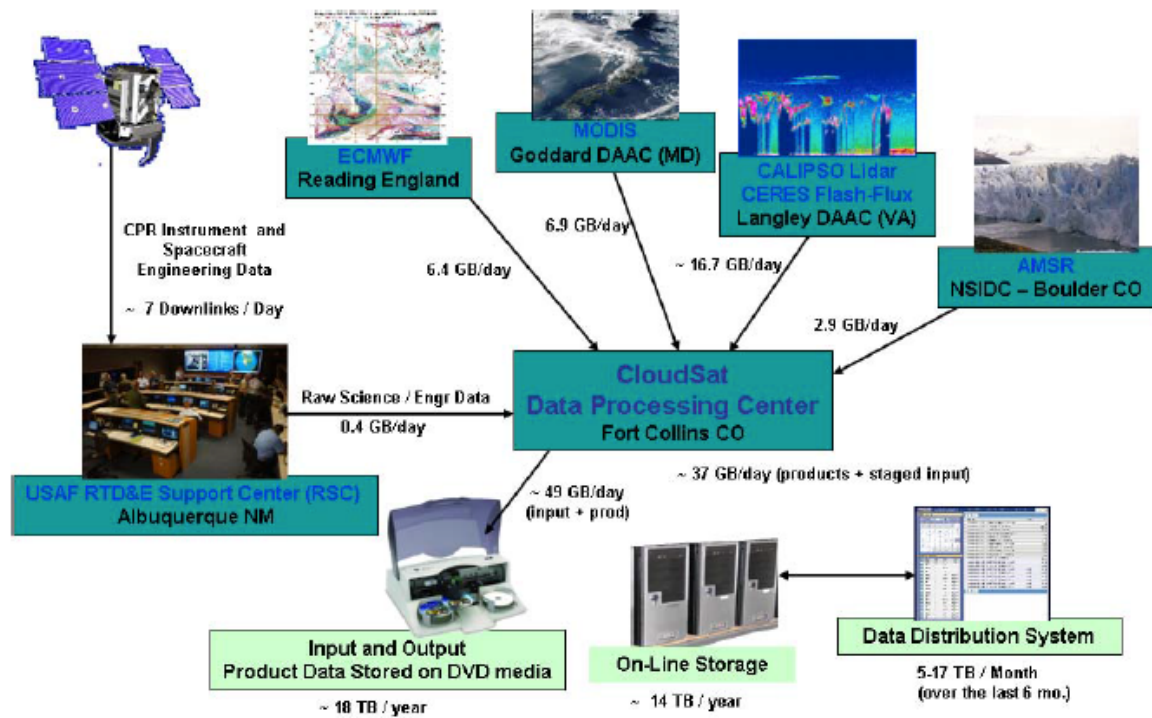


Figure 2. CloudSat System Data Flow (from Cooperative Institute for Research in the Atmosphere 2008)

CloudSat Science and Engineering Data are downlinked from the CloudSat onboard data recorder through the Air Force Satellite Communications Network (AFSCN) to the USAF RDT&E Support Center (RSC) in Albuquerque, NM. There, the

raw data are decommutated, checked for transmission errors, and stored online as a set of binary files. The raw data can then be accessed by the CloudSat Data Processing Center via internet/ftp for necessary level zero through two processing centers (Cooperative Institute for Research in the Atmosphere (CIRA), 2008) .

C. CLOUD PROFILING RADAR

The CPR onboard CloudSat employs a technology similar to a ground-based weather radar but at a much more sophisticated level. The CPR utilizes a 94-GHz nadir looking millimeter wavelength radar. Ground-based weather radars employ a centimeter wavelength band, enabling detection of raindrop-size particles. The increased sensitivity of the CPR has allowed scientists the ability to study the interior structure of clouds and the processes within them. The CPR system characteristics are defined in Table 2.

Table 2. CPR System characteristics.

Frequency	94 GHz
Altitude	705 km
Vertical Resolution	500 m
Cross-track Resolution	1.4 km
Along-track Resolution	1.7 km
Pulse Width	3.3 μ sec
Pulse Repetition Frequency	4300 Hz
Minimum Detectable Z[*]	- 28 dBZ

The CPR measures the power backscattered by the clouds as a function of distance from the radar. In a Rayleigh regime, such as cloud particles that are small relative to the radar's wavelength, the cloud reflectivity increases as λ^4 , where λ represents the radar wavelength. The design of the CPR was driven by the primary science objective, which was a minimum detectable cloud reflectivity (Z) of at least -26 dBZ. For comparison, the 14-GHz Tropical Rainfall Measuring Mission (TRMM) Precipitation Radar (PR) has a sensitivity of +20 dBZ, as it is primarily designed to detect rainfall, which generally has reflectivity values of 20-50 dBZ. A hurdle in determining the optimal frequency is atmospheric attenuation, which becomes much more restrictive at higher frequencies. The nominal frequency of 94-GHz was chosen from these

considerations, which in turn provided an increase of 33 dBZ over the use of the 14-GHz operating frequency of TRMM PR.

CloudSat is flown in a sun-synchronous orbit at an altitude of 705 km and an along-track velocity of 7 km sec^{-1} . At this velocity, the CPR onboard CloudSat generates a profile every 1.1 km along its track. Each profile has 125 vertical bins and is approximately 240 m thick. This results in an along-track resolution of 1.7 km and a cross-track resolution of 1.4 km.

D. ESTIMATING TROPICAL CYCLONE INTENSITY

Over much of the world, TC intensity and structure are estimated nearly entirely on satellite-based technology, with the exception of the Atlantic Ocean and Gulf of Mexico near the United States where airborne reconnaissance is still in operation. As such, forecasters at JTWC rely on satellite technology to predict TC structure and intensity.

The first technique to successfully and accurately estimate the intensity of a TC in an environment where aircraft reconnaissance was not present was described by Dvorak (Velden et al., 2006) . The Dvorak technique was based on a revolutionary conceptual model of TC development and decay, which derived an empirical method relating TC cloud structures to storm intensity using a simple numerical index corresponding to an estimate of the maximum sustained surface wind (MSW) (Velden et al., 2006). Dvorak went on to update the technique in 1973, 1975, and 1984. It has remained in operational use to this day, compiling over four decades of enabling forecasters and saving a countless number of lives in the process.

Utilizing satellite technology such as the A-Train constellation, the potential exists once again to revolutionize the manner in which forecasters utilize satellite capabilities to better predict storm intensity and structure. In WE2007, storm intensity is estimated as a function of structural characteristics that represent the energy and thermodynamic efficiency of the storm. Cloud-top parameters are used to represent TCs are in a quasi-steady state mature TC. The study used a balanced vortex model and asymmetry of a quasi-steady state. Model-derived parameter of cloud and

thermodynamic properties was identified as input to the TC intensity estimate scheme. In the WE2007 model, a TC is an approximately axisymmetric vortex, very nearly in a state of hydrostatic and gradient wind balance. Furthermore, WE2007 developed a relationship between the change in saturation entropy, maximum wind speed, and pressure drop between the storm center and its environment. This equation is based on Emanuel (1986) that defined a specific relationship between the distributions of angular momentum per unit mass, M , and saturation entropy, s^* , given by

$$MdM = -r^2(T_s - T_o)ds^* \quad (1)$$

where r is the radial distance from the storm rotation axis, T_s is the absolute surface temperature, T_o is the saturation entropy-weighted absolute temperature of the storm top. The angular momentum per unit mass and saturation entropy are defined as,

$$M \equiv rV + \frac{1}{2}fr^2 \quad (2)$$

and

$$s^* \equiv C_p \ln(T) - R_d \ln(p) + \frac{L_v q^*}{T} \quad (3)$$

Here, V is the azimuthal velocity, f is the Coriolis parameter, C_p is the heat capacity at constant pressure, R_d is the gas constant for dry air, p the pressure, L_v the latent heat of vaporization, and q^* is the saturation specific humidity. Using (1), (2), and (3), WE2007 developed an expression for the maximum wind speed, V_m given by

$$V_m^2 \equiv \frac{\left(\frac{T_s - T_o}{T_o}\right) \Delta h^* - \frac{1}{4} f^2 r_o^2}{\frac{R_d T_s}{36 p_o} - 1} \quad (4)$$

In equation (4) Δh^* is the total change of saturation moist static energy from the eyewall to the environment, and p_o is the surface pressure at a radius r_o where the surface wind is assumed to vanish and the TC blends into the environment. In WE2007 a high resolution model was used to relate TC intensity to the difference between the moist static energy, h^* , of the eyewall and that of the undisturbed environment Δh^* , and to the difference between the absolute temperatures of the boundary layer T_s and of the storm top T_o .

Their ultimate goal was to estimate the intensity of real TCs using satellite borne cloud radar to detect cloud top height and infrared radiometers to estimate cloud top temperatures. If sufficiently accurate estimates of cloud top height across the eyewall T_o can be made, and if there are sufficiently accurate estimates of the sea-surface temperature T_s and temperature at the outflow level, one can attempt to use (4) to estimate storm intensity.

In the nineteenth century French physicist Carnot, published the concept of an efficient heat engine. Posthumously, he became known as the father of thermodynamics. Emanuel (2005) applied the concept of a Carnot cycle to TCs as a way to explain the thermodynamic efficiency of utilizing the heat input to the storm from the ocean. The cycle seen in Figure 3 depicts an air parcel initially traveling along the sea surface. On leg A-B, the parcel is traveling toward the lower pressure near the eyewall. The proximity to the sea surface, which acts as a heat reservoir, provides heat input to keep the parcel near a constant temperature, but provides for an increase in its moisture content. Additionally, the parcel expands as it flows toward the low pressure of the storm center. At point B, the air parcel undergoes very rapid adiabatic ascent as it meets the strong updrafts of the cumulonimbus that make up the eyewall. The latent heat gathered in the leg A-B is converted into sensible heat as water vapor condenses. This provides the warm core at the storm center that contributes to low surface pressure and increasing surface wind speeds. At point C, the temperature of the parcel has cooled to be that of the environment. The parcel undergoes isothermal compression on the relatively short leg C-D as the parcel leaves the storm to be incorporated into the surrounding environment. Finally, the parcel experiences adiabatic compression as it descends during leg D-A. (Emanuel, 2005)

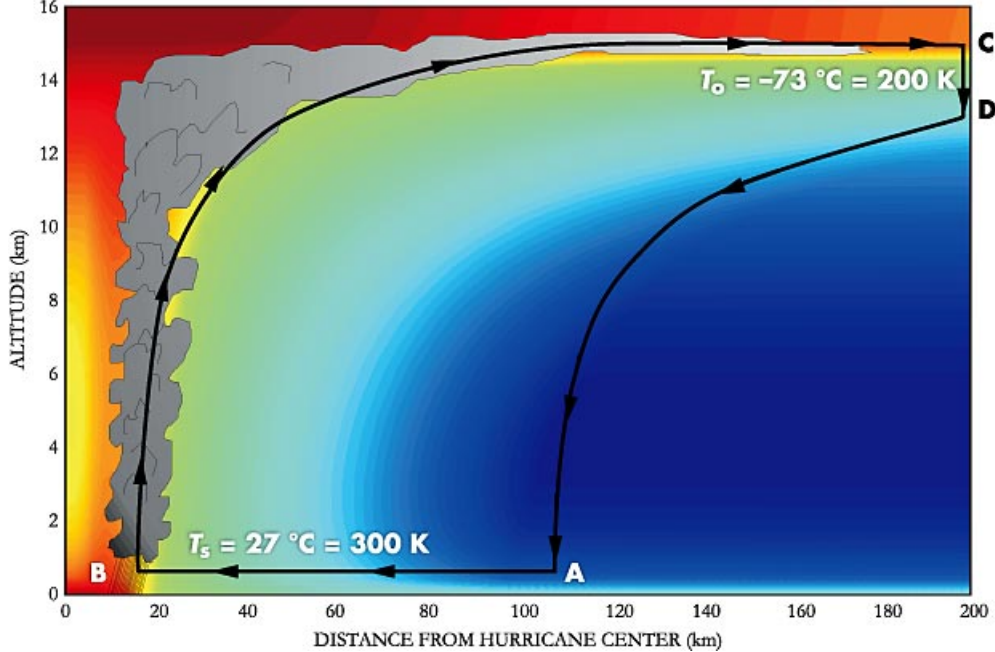


Figure 3. The energy cycle of a mature TC (from Emanuel 2005)

Using the Carnot cycle framework, Luo et al. (2008) applied the techniques developed by WE2007 to CloudSat TC data from 2006–2007 to modify Eq. (4) such that cloud-top temperature, cloud-top height, and surface temperature could be used to compare estimated TC intensity. Luo et al. (2008) approximated Eq. (4) as shown below.

$$V_m^2 \approx \left(\frac{T_s - T_o}{T_o} \right) \Delta h^* \quad (5)$$

As in Eq. (4), Δh^* is a measure of the difference in moist static energy between the TC core and surrounding environment. Here moist static energy is defined as

$$h^* = C_p T + gZ_c + L_v q^* \quad (6)$$

Luo et al. (2008) assumed that temperature variations with altitude are small in the lower stratosphere and at these very low temperatures the contribution of latent heat to moist static energy is negligible.

Luo et al. (2008) compared the estimated TC intensity using Eq. (5) to the best-track data. The limitation of the WE2007 method was the requirement of an eye or near-eye overpass, which reduced the number of TCs that could be included in the study. Luo

et al. were only able to consider nine cases at the time of their study. Therefore, the Luo et al. (2008) calculations were based on estimating Δh^* in Eq. (4) by assuming that variations in moist static energy along the cloud tops were dominated by variations in potential energy (gZ_c). Therefore, stronger TCs would have steeper cloud-top slopes from the eyewall to an outer rainband. The downward slope in cloud-top height from the eyewall to the outer rainbands can be understood as a manifestation of the change of saturation moist static energy, h^* .

To test the validity of using cloud-top height difference as a proxy for Δh^* , Luo et al. (2008) computed V_m using Eq. (5) by calculating h^* explicitly and compared that to V_m that resulted from using cloud-top height. To calculate h^* , they used SST values at the storm center and assumed an 80% relative humidity for the environmental h^* . Luo et al. summarized the two methods by plotting the estimated maximum wind against the best track maximum sustained winds (Figure 4). The dots are cases in which Δh^* was calculated explicitly and triangles are represent cases in which CloudSat cloud-top height data were employed to estimate Δh^* .

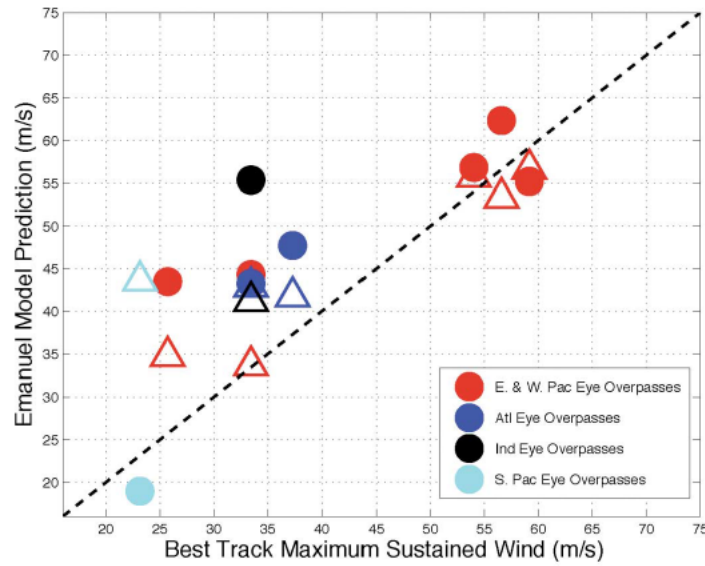


Figure 4. Estimated versus best track “observed” tropical storm intensity. Triangles define cases in which CloudSat data were used and circles define cases in which Δh^* was calculated explicitly
(from Luo et al. 2008b)

In their study, Luo et al. found that there was some agreement attained for stronger storms vice weaker ones. Both methods provided estimated maximum winds that were too high for weaker TCs. However, the SST technique tended to have larger overestimates of the maximum sustained wind for weaker TCs. They noted that one degree of error in SST would translate into 18-35 % of error in the estimated maximum sustained wind. As a result of this shortcoming, they recommended moving away from using SST as a basis for estimating the environmental moist static energy. In conclusion, Luo et al. recommended further examination into the method and a larger data set, which is what this current study intends to accomplish.

Given the relative success provided by use of the CloudSat data estimating Δh^* in Eq. (5), this thesis is aimed at increasing the sample size from that of Luo et al. (2008). Additionally, sensitivities to overpass distance to the TC estimate, storm intensity, and storm structure are investigated.

THIS PAGE INTENTIONALLY LEFT BLANK

III. METHODOLOGY

A. DATA

1. Data Source

Through an agreement between Naval Research Laboratory (NRL) and the CloudSat DPC, whenever a CloudSat overpass intersects a TC within 1000 km a CloudSat overlay of radar reflectivity is created using MODIS, AMSR-E, and other satellite imagery. The NRL display includes the 3-D cross-sectional analysis atop a 2-D satellite image product (Mitrescu et al., 2008). An example overlay of the CPR measured reflectivity and AQUA image for Typhoon (TY) Choi-Wan in 2009 is provided in Figure 5.

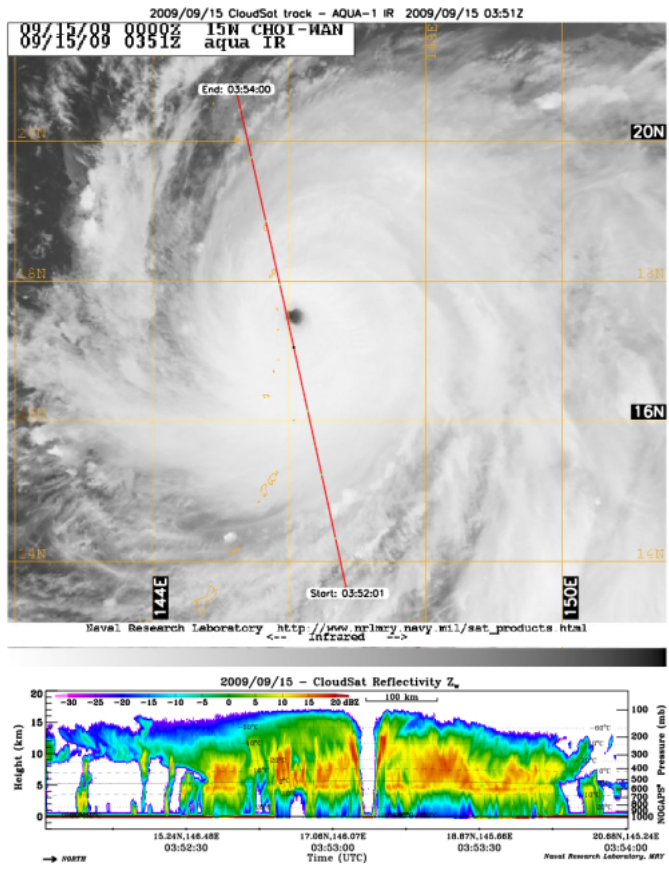


Figure 5. NRL produced overlay of CHOI-WAN from 15 SEP 2009. The upper panel is an infrared image at 0351 UTC and the lower image is a radar cross section taken along the red line in the upper panel. (from Colorado State University 2014).

The data for this study consist of TCs in the WPAC from 2006–2013. The dataset is limited to TCs that CloudSat and the other members of the A-Train constellation were in position to successfully overpass. Since launch, nearly 8,000 overpasses of tropical storms have been collected within 1000 km of the storm center. However, the WE2007 method requires an eye or near-eye overpass, which limits the volume of cases that can be considered. The overpasses are stratified by distance from the storm center in Table 3.

Table 3. CloudSat TC Overpasses by Distance from 2006–2013.

TC Overpasses by Distance	Count
≤ 50 km	114
≤ 100 km	216
≤ 150 km	333

For the purpose of this study, only overpasses within 50 km of the storm center were considered. Of the 114 overpasses within 50 km, 65 of them have full coverage of parameters suitable for the WE2007 method. The TCs are further stratified by year (Table 4) and intensity based on the Saffir-Simpson scale (Table 5). The largest number of TC overpasses within 50 km occurred during 2009. In April 2011, CloudSat suffered a battery anomaly resulting in the satellite being removed from the A-Train constellation. During May 2012, CloudSat successfully reentered the A-Train constellation, 394 days after the battery anomaly and 333 days after dropping out of the A-Train constellation. However, operation was limited to daytime hours only. The battery anomaly resulted in no exploitable data in 2011 and a decrease in 2012.

The majority of the TCs used for the study were below typhoon strength. However, of those that reached typhoon strength most of them were category one status. There is representation from all five categories of the Saffir-Simpson scale. The strongest typhoon occurred in September 2006 reaching 140 kt at the time of overpass.

Table 4. CloudSat TC statistics by year.

TC Statistics 2006-2013	Count
2006	13
2007	14
2008	14
2009	20
2010	0
2011	0
2012	4
2013	0
TOTAL	65

Table 5. CloudSat TC statistics from 2006-2013 based on Saffir-Simpson scale.

TC Statistics 2006-2013	Count
Tropical Depression	19
Tropical Storm	17
Category 1	14
Category 2	4
Category 3	6
Category 4	4
Category 5	1

The complete dataset is provided in Table 6. Here the data are arranged by ascending minimum distance (km) from the pass of the A-Train constellation to the storm center. There are divisions marking each 10 kilometers of the dataset. The first third of the data have a minimum distance of less than 18 km.

Table 6. CloudSat TC Overpasses arranged by Minimum Distance.

NAME	DATE	NBR	MIN DIST (km)	TYPE	INTENSITY (KT)	WIND (m/s)
DURIAN	12/1/2006	24W	0.5	CAT1	80	41.2
NONAME	8/3/2007	06W	2.3	TD	30	15.4
PRAPIROON	8/2/2006	07W	3.3	CAT1	65	33.4
KETSANA	9/27/2009	17W	4.5	TS	55	28.3
NANGKA	6/25/2009	04W	5.3	TS	45	23.1
EIGHTEEN	9/28/2009	18W	7.6	TD	30	10.3
NIDA	11/30/2009	26W	8.3	CAT3	100	51.4
CHEBI	11/10/2006	23W	10.4	CAT4	125	59.2
KAJIKI	10/21/2007	19W	10.9	CAT4	115	48.9
USAGI	7/29/2007	05W	11.0	CAT1	65	33.4
MELOR	10/9/2009	20W	13.0	TS	45	23.1
GAEMI	10/5/2012	21W	13.6	TS	35	18.0
NARI	9/11/2007	12W	14.7	TD	20	7.7
PRAPIROON	7/30/2006	07W	15.3	TD	20	12.9
WUKONG	8/14/2006	11W	15.9	TS	50	25.7
MELOR	10/8/2009	20W	16.1	TS	45	25.7
KROVANH	8/31/2009	12W	16.2	TS	55	23.1
MEKKHALA	9/29/2008	20W	17.0	TS	40	20.6
NIDA	11/28/2009	26W	17.3	CAT4	125	66.9
NONAME	11/26/2007	25W	17.9	TD	25	12.9
BILIS	7/8/2006	05W	18.0	TD	30	15.4
FUNG-WONG	7/25/2008	09W	18.2	TS	35	18.0
KONG-REY	3/31/2007	01W	18.4	TD	25	10.3
UTOR	12/10/2006	25W	18.6	CAT1	65	46.3
FUNG-WONG	7/29/2008	09W	18.8	TD	20	12.9
JANGMI	9/25/2008	19W	19.8	CAT1	80	41.2
WUKONG	8/17/2006	11W	20.0	TS	55	23.1
LINGLING	10/14/2007	18W	21.3	TS	35	15.4
NAKRI	6/2/2008	06W	21.3	CAT2	85	38.6
KUJIRA	5/6/2009	01W	21.3	CAT3	100	51.4
LUPIT	10/21/2009	22W	22.1	CAT1	75	41.2
KAMMURI	8/5/2008	10W	22.7	TS	45	23.1
CHOI-WAN	9/15/2009	15W	23.3	CAT4	130	66.9
MAYSAK	11/6/2008	24W	23.5	TD	30	18.0
MARIA	10/19/2012	23W	25.1	TD	30	15.4
EIGHTEEN	9/28/2009	18W	26.0	TD	30	15.4
NARI	9/16/2007	12W	27.0	CAT1	75	38.6

NAME	DATE	NBR	MIN DIST (km)	TYPE	INTENSITY (KT)	WIND (m/s)
KALMAEGI	7/19/2008	08W	28.1	TD	30	15.4
NONAME	7/4/2006	04W	28.2	CAT3	110	56.6
FRANCISCO	9/22/2007	15W	28.8	TD	25	12.9
SINLAKU	9/7/2008	15W	29.0	TD	20	12.9
LUPIT	10/16/2009	22W	30.6	CAT1	80	33.4
USAGI	7/28/2007	05W	30.9	TD	20	10.3
MITAG	11/24/2007	24W	31.2	CAT2	85	43.7
VAMCO	8/22/2009	11W	31.9	CAT3	110	48.9
NURI	8/16/2008	13W	32.5	TS	50	7.7
TWENTY-SEVEN	11/22/2009	27W	33.3	TD	20	12.9
LINFA	6/16/2009	03W	33.7	TD	20	10.3
UTOR	12/13/2006	25W	34.0	CAT1	60	33.4
PEIPAH	11/4/2007	21W	37.4	CAT1	65	33.4
KALMAEGI	7/12/2008	08W	37.8	TD	20	10.3
PARMA	9/30/2009	19W	38.4	CAT3	105	51.4
NAKRI	5/31/2008	06W	39.0	CAT2	95	36.0
YAGI	9/21/2006	16W	39.9	CAT5	140	72.0
DURIAN	12/4/2006	24W	41.5	CAT1	50	25.7
HIGOS	9/30/2008	21W	42.2	TS	40	23.1
JELAWAT	9/29/2012	18W	43.0	CAT3	100	51.4
FITOW	9/4/2007	10W	43.1	CAT1	75	38.6
GONI	8/3/2009	08W	44.0	TD	30	15.4
SANVU	5/27/2012	03W	46.1	TS	50	25.7
HAGUPIT	9/21/2008	18W	46.6	CAT1	80	38.6
CIMARON	10/30/2006	22W	47.2	CAT2	90	46.3
MIRINAE	10/31/2009	23W	47.7	TS	55	28.3
TWENTY-FIVE	11/8/2009	25W	48.5	TS	45	23.1
PABUK	8/7/2007	07W	49.4	CAT1	65	33.4

2. Data Format

The raw CloudSat TC overpass data are cataloged by the CloudSat Data Processing Center (DPC) and available for public access in Hierarchical Data Format (HDF). The format HDF is the prescribed format for standard data products derived from NASA Earth Observing System (EOS) missions. The HDF data format is particularly useful for management and preservation of large and complex scientific datasets such as those held by NASA's Earth Observing System Data and Information System (EOSDIS)

(Brennan et al., March-April 2013). The HDF files allow for ease of access to data products and fields measured by CloudSat and other members of the A-Train.

3. CloudSat Products

The CloudSat sun-synchronous orbit and speed allow for 15 orbits per day. Each orbit is known as a granule and results in a repeat of the ground-track every 16 days. These granules are defined as one orbit and contain standard and auxiliary data products that are processed by the CloudSat DPC. A HDF data file containing the overpass time, reflectivity, AMSR-E, and environmental parameters from the Navy operational model, NAVGEM, is created and transferred through the automated system at NRL ten days after the overpass. The standard and auxiliary data products are detailed in Table 7. The primary product is the level-1B calibrated, range-resolved radar reflectivities and the essential level-2 products are the cloud profile properties derived from these radar data (Stephens et al., 2002).

Table 7. List of CloudSat level-1 and level-2 products
(after Stephens et al. 2002)

Product ID	Description	Principal inputs	Characteristics and references
Standard products			
IA-AUX	Auxiliary data for navigation altitude assignments, raw CPR data.	Digital elevation maps, spacecraft ephemeris.	
IB-CPR	Calibrated radar reflectivities.	Radar power, calibration factors.	500-m vertical resolution; day and night.
2B-GEOPROF	Cloud geometric profile—expressed in terms of occurrence and reflectivity (significant echoes), also includes (gas) attenuation correction.	IB-CPR, AN-MODMASK. A modified version of this product that includes CALIPSO lidar data is planned.	500-m vertical resolution (but the lidar-radar product will have higher vertical resolution); day and night.
2B-CLDCLASS	Eight classes of cloud type, including precipitation, identification, and likelihood of mixed phase conditions.	Radar and other data from the constellation.	Wang and Sassen (2001); day and night.
2B-TAU	Cloud optical depth by layer.	2B-GEOPROF and MODIS-AUX radiances.	$\tau > 0.1$, 20% accuracy (goal); daytime only.
2B-LWC	Cloud liquid water content.	2B-GEOPROF and 2B-TAU.	500 m and 50%; day and night, daytime uses 2B-TAU, nighttime product will be inferior to daytime.
2B-IWC	Cloud ice water content.	2B-GEOPROF and 2B-TAU, temperature	500 m +100% to -50%; day and night; daytime product uses 2B-TAU, nighttime product is inferior to daytime product.
2B-FLXHR	Atmospheric radiative fluxes and heating rates.	2B-GEOPROF, 2B-TAU, 2B-LWC/IWC.	Resolve longwave fluxes at TOA and surface to $\sim 10 \text{ W m}^{-2}$ and equivalently in cloud heating $\sim \pm 1 \text{ K day}^{-1} \text{ km}^{-1}$.
Auxiliary data			
MODIS-AUX	MODIS radiances and cloud mask.	Radiances from 23 of the MODIS channels $\pm 35 \text{ km}$ about CloudSat ground track.	
AN-STATVAR	Subset along track of forecast model state variables.	The subsetting details are currently under study.	
AN-AMSR	AMSR-E radiances		
Selected experimental products			
Precipitation	Quantitative precipitation.	2B-GEOPROF and AN-AMSR radiances.	
Cloud phase	Discrimination of ice and liquid.	2B-GEOPROF, CALIPSO lidar, MODIS radiances.	
Cloud microphysics	Droplet size profiles, number concentrations.	2B-GEOPROF, 2B-TAU, CALIPSO lidar, MODIS radiances.	

a. **2B-GEOPROF**

Conventional satellite data have allowed only approximate measures of the location and vertical extent of clouds. The 2B-GEOPROF product, of the active remote

sensing CloudSat, is the cloud geometrical profile that produces an estimate of the radar reflectivity factor for the levels in the vertical column that contain a significant echo. It is also known as the “Cloud Mask,” as it provides the first product to deliver a field that indicates the presence of a cloud inside a CPR bin. This product was instrumental in supplying fields such as profile time, latitude, longitude, height, and reflectivity.

b. MODIS-AUX

The MODIS-AUX data set is an intermediate product that contains a subset of ancillary MODIS radiance and cloud mask data that overlaps and surrounds each CloudSat CPR footprint (Cooperative Institute for Research in the Atmosphere (CIRA), 2008). The associated algorithm uses reference and independent geolocation data to find the closest MODIS pixel to the CloudSat ray, and then stores it in a 21-pixel across-track by 5-pixel along-track grid of each parameter of interest resulting in a 105-element vector. This product supplied such fields as cloud top height, cloud top temperature, and brightness temperature.

4. CloudSat Fields

Each HDF file produced by NRL contains geolocation and data fields, defined in Tables 8 and 9. The bold fields within these two tables represent those specifically employed in this study. The geolocation fields (Table 8) utilize the 2B-GEOPROF standard data product and provide information to the user regarding the storm-centered position, track, and best track data.

Table 8. Listing of geolocation fields within a characteristic HDF File.

Parameter	Units	Data Source/Description
StormCenterLat	degrees	Best Track
StormCenterLon	degrees	Best Track
Storm MSLP	<i>mb</i>	<i>Best Track</i>
StormMaxWind	m/s	Best Track
ProfileTime	<i>seconds</i>	2B-GEOPROF
Latitude	<i>degrees</i>	2B-GEOPROF
Longitude	<i>degrees</i>	2B-GEOPROF
LandSeaFlag	1, 2, or 3	2B-GEOPROF

Parameter	Units	Data Source/Description
Date_Created	yr, mon, day, hr, -- min, secs (MST)	
Min_Radial_Dist	km	<i>Minimum distance of CS point to TC center</i>
Other_BestTrackData	--	Array of before/after best track overpass data
Storm_Shear	knots	SHIPS
Storm_Center_SST	C	Reynolds

The data fields (Table 9) contain most of the standard data products. These data fields provided graphical and numerical information that define the storm intensity.

Table 9. Listing of data fields within a characteristic HDF file. Bold entries were used in this study.

Data Field	Units	Data Source
PressLevels	mb	NoGAPS
Temperature	K	NoGAPS
HeightLevels	km	NoGAPS
Dewpoint	K	NoGAPS
Usfc	m/s	NoGAPS
Vsfc	m/s	NoGAPS
Tairsfc	K	NoGAPS
SST	K	NoGAPS
89H_Brightness_Temp_NRL	K	NRL AMSR-E data
SST_AMSRE_NRL	K	NRL AMSR-E data
Wind_AMSRE_NRL	m/s	NRL AMSR-E data
Water_vapor_AMSRE_NRL	km/m ²	NRL AMSR-E data
LWP_AMSRE_NRL	km/m ²	NRL AMSR-E data
Rain_rates_AMSRE_NRL	mm/h	NRL AMSR-E data
Radial_Dist	km	--
Height	m	2B-GEOPROF
Cloud_Mask	--	2B-GEOPROF
Gaseous_Attenuation	dBZ	2B-GEOPROF
Reflectivity	dBZ	2B-GEOPROF
Cloud_Top_Height	m	MOD06-5KM-AUX
Radius	km	--
Azimuth	degrees	--
Surface_Height_Bin	--	2B-GEOPROF
Cloud_Top_Temp	K	MOD06-5KM-AUX

Data Field	Units	Data Source
Cloud_Top_Press	hPa	MOD06-5KM-AUX
Brightness_Temp	K	MOD06-5KM-AUX
Precip_rate	mm/h	2C-PRECIP-COLUMN
Precip_rate_min	mm/h	2C-PRECIP-COLUMN
Precip_rate_max	mm/h	2C-PRECIP-COLUMN
Precip_rate_no_ms	mm/h	2C-PRECIP-COLUMN
Near_surface_reflectivity	dBZe	2C-PRECIP-COLUMN
Lowest_sig_layer_top	km	2C-PRECIP-COLUMN
Highest_sig_layer_top	km	2C-PRECIP-COLUMN
Frozen_precip_height	km	2C-PRECIP-COLUMN
Melted_fraction	--	2C-PRECIP-COLUMN
Precip_flag	--	2C-PRECIP-COLUMN
Cloud_flag	--	2C-PRECIP-COLUMN
Surface_type	--	2C-PRECIP-COLUMN
Freezing_level	km	2C-PRECIP-COLUMN
SST	C	2C-PRECIP-COLUMN
Surface_wind	m/s	2C-PRECIP-COLUMN
CLWP	g/m ²	2C-PRECIP-COLUMN
RLWP	g/m ²	2C-PRECIP-COLUMN
Conv_strat_flag	--	2C-PRECIP-COLUMN
PIA_hydrometeor	dB	2C-PRECIP-COLUMN
Rain_top_height	km	2C-PRECIP-COLUMN
Ice_Water_Content	mg/m ³	2B-CWC-RO
Ice_Water_Path	g/m ²	2B-CWC-RO
RO_ice_effective_radius	μm	2B-CWC-RO
RO_ice_number_conc	cm ⁻³	2B-CWC-RO
RO_ice_distrib_width_param	--	2B-CWC-RO
Cloud_scenario	--	2B-CLDCLSS
ECMWF_Temperature	K	ECMWF-AUX
ECMWF_Pressure	Pa	ECMWF-AUX
ECMWF_Specific_humidity	kg/kg	ECMWF-AUX
ECMWF_Temperature_2m	K	ECMWF-AUX
LIDAR_CloudFraction	--	2B-GEOPROF-LIDAR
LIDAR_UncertaintyCF	--	2B-GEOPROF-LIDAR
LIDAR_CloudLayers	--	2B-GEOPROF-LIDAR
LIDAR_LayerBase	m	2B-GEOPROF-LIDAR
LIDAR_LayerTop	m	2B-GEOPROF-LIDAR
LIDAR_FlagBase	--	2B-GEOPROF-LIDAR
LIDAR_FlagTop	--	2B-GEOPROF-LIDAR

5. Measuring Δh^*

During their study, Luo et al. employed two methods to estimate storm intensity. The first method was based on cases where equation (6) was calculated explicitly. The procedure used the idea that the saturation moist static energy at the tops of the outer convective clouds, h_o^* , will be approximately equal to the actual moist static energy of undisturbed air in the boundary layer. This method employed extrapolated SST and 80 % relative humidity for estimating the environmental h_o^* . The second method for predicting storm intensity estimated the moist static energy, Δh^* , using only CloudSat data. This procedure, using only CloudSat data, assumes the contribution to Δh^* comes mainly from the difference in cloud-top height, seen in Figure 6 as the downward slope of cloud tops from the inner core near the eyewall to outer rainbands.

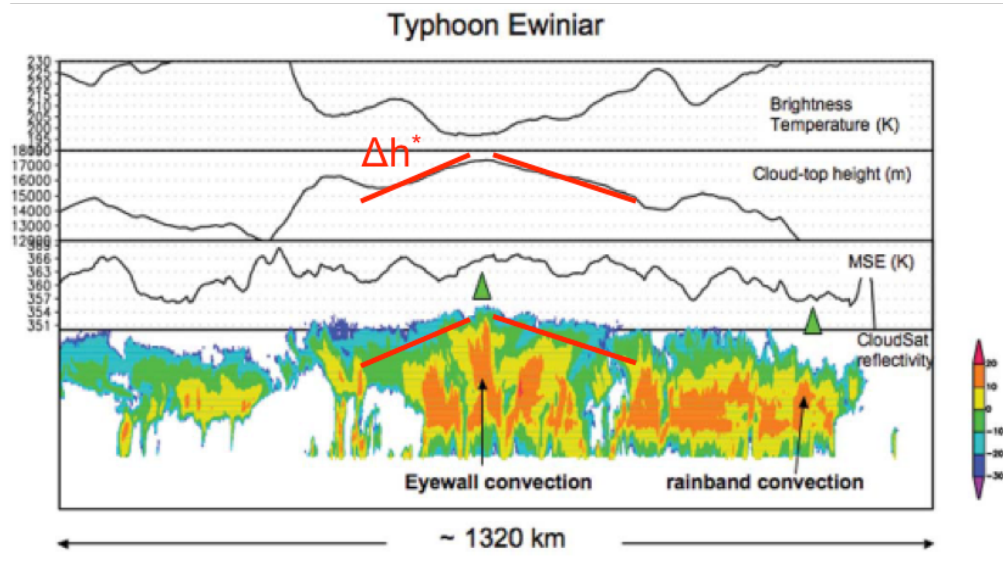


Figure 6. Typhoon Ewinar: (from top to bottom) 11- μ m brightness temperature (in kelvins), cloud-top height (in meters), calculated moist static energy (in Kelvin), and CloudSat reflectivity (in decibels referenced to zero) (after Luo et al. 2008b).

Luo et al. (2008b) noted that it is not always possible to identify representative convective cores in the spiral bands, especially since there is no guarantee that CloudSat will intersect such convection. Therefore, Luo et al. chose a representative outer rainband to define the outer location from which the cloud-top slope should be computed.

The location of an outer rainband is subjectively determined. Additionally, another rainband may not be evident if the overpass is far from the center. With these points in mind, this thesis defines an objective measure for estimated Δh^* , described below.

Figure 7 displays an example CloudSat reflectivity distribution for Typhoon Choi-Wan from 2009. The red dashed line in the second subplot represents zero dBZ. For calculation of cloud-top slope the outer location is defined by calculating the difference in cloud-top height from the highest clouds near the TC center to the related location where reflectivity first becomes zero dBZ. The measure of h^* was defined from the cloud-top height on each side of the center of the TC, or the closest point of approach between the satellite overpass and the storm center. These values were then averaged before input into Eq. (5) as Δh^* , which produced an estimated value for the maximum sustained wind.

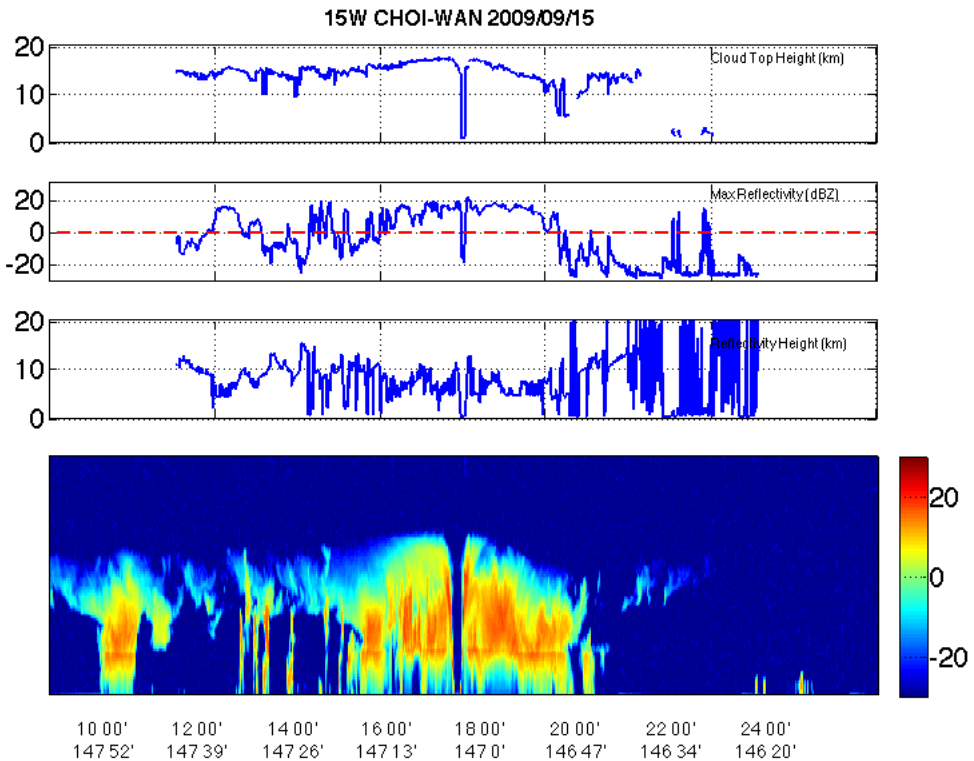


Figure 7. Typhoon Choi-Wan (from top to bottom) cloud-top height (in km), max reflectivity (in dBZ), height of max reflectivity (in km), and CloudSat reflectivity (in dBZ).

IV. ANALYSIS AND RESULTS

A. ANALYSIS

Once the total set of TC cases was reduced to 65, data defined in Table 9 were extracted from each granule. The variables as defined in Table 9, relevant to this study include sea-surface temperature, cloud-top temperature, cloud-top height, reflectivity, storm max wind, minimum distance to the storm center, and shear.

The storm maximum wind and reflectivity data products were used to categorize the dataset by TC intensity. The reflectivity array was used to categorize the intensity by finding the maximum reflectivity value for each of the 125 vertical bins in the path over the storm. The maximum of the resultant array was used to define the highest recorded reflectivity, in dBZ, within the granule. The storm maximum wind was used to categorize the TC intensity by comparing this information to the archive best track data provided on the JTWC website. The storm maximum wind and best track data were used to provide a sequence in TC intensity from the overpass time minus 12 hours to overpass plus 6 hours. This provided a measure of whether the storm was intensifying or weakening. However, analyses of these parameters in relation to the estimated maximum wind reveal no impact due to storm change in intensity.

The calculations performed utilized equation (5), which neglects the earth angular momentum and a factor related to the surface pressure deficit terms seen as the third and fourth terms of equation (4). The inflow temperature, T_s , was defined by the surface temperature, which was assumed to be equal to the sea-surface temperature. The outflow temperature, T_o , was defined by cloud-top temperature provided within the MODIS data and *Aqua*. The next variable, Δh^* , is the total change of saturation moist static energy from the eyewall to the environment. As defined above by Luo et al. (2008), Δh^* was calculated from the cloud-top height at the center of the TC outward in both directions to a point where the CPR observed a reflectivity value of zero decibels.

In this study the sensitivity of calculated maximum wind is defined relative to the overpass distance to the TC center, the TC intensity, and the TC structure deviation due

to vertical wind shear. The TC overpasses that possessed a clear storm center (i.e. well-defined eye) are separated as a subset of cases to identify the best signal in which the value of cloud-top height could be used to calculate the total moist static energy. The cases characterized by having a clear center contained 22 TCs, or approximately one-third of the data set and is defined in Table 10 by the Saffir-Simpson intensity index.

Table 10. CloudSat TC statistics from 2006-2013 of cases containing a clear center stratified by Saffir-Simpson scale.

TC Statistics 2006-2013	Count
Tropical Depression	3
Tropical Storm	1
Category 1	6
Category 2	2
Category 3	5
Category 4	4
Category 5	1

B. COMPARISON AGAINST BEST TRACK DATA

The calculated maximum wind speed for all cases in Table 6 are presented below in Table 11 with those 22 TCs that contain a clear center highlighted by bold-italic font. The data are arranged in chronological order by date. The best track intensities (column 4) are from the JTWC Best-Track archive at the 6 h point closest to the satellite overpass, and the maximum wind data points are from the data field contained in the HDF file and define the wind speed at the time of satellite overpass. The Vmax column contains the calculated maximum sustained wind using Eq. (5). The last column labeled intensity diff is the disparity between calculated maximum sustain wind and the maximum wind at the time of the satellite overpass. The positive values in this column represent an over estimation and negative values represent an under estimation of the maximum sustained wind against the best track estimation.

Table 11. Intensity prediction based on CloudSat and A-Train measurements.

Name	Date	Type	Intensity (kt)	Min Dist (km)	Max Wind (m/s)	Vmax (m/s)	Intensity Diff [Vmax - BT]
<i>NONAME</i>	7/4/2006	CAT3	110	28.2	56.6	35.3	-21.3
BILLIS	7/8/2006	TD	30	18.0	15.4	53.9	38.5
PRAPIROON	7/30/2006	TD	20	15.3	12.9	27.1	14.2
<i>PRAPIROON</i>	8/2/2006	CAT1	65	3.3	33.4	31.8	-1.6
WUKONG	8/14/2006	TS	50	15.9	25.7	NaN	NaN
<i>WUKONG</i>	8/17/2006	TS	55	20.0	23.1	28.4	5.3
<i>YAGI</i>	9/21/2006	CAT5	140	39.9	72.0	29.4	-42.6
CIMARON	10/30/2006	CAT2	90	47.2	46.3	29.7	-16.7
<i>CHEBI</i>	11/10/2006	CAT4	125	10.4	59.2	46.6	-12.7
DURIAN	12/1/2006	CAT1	80	0.5	41.2	30.7	-10.5
DURIAN	12/4/2006	CAT1	50	41.5	25.7	38.4	12.7
UTOR	12/10/2006	CAT1	65	18.6	46.3	28.2	-18.1
UTOR	12/13/2006	CAT1	60	34.0	33.4	NaN	NaN
KONG-REY	3/31/2007	TD	25	18.4	10.3	34.4	24.1
USAGI	7/28/2007	TD	20	30.9	10.3	26.7	16.4
USAGI	7/29/2007	CAT1	65	11.0	33.4	34.3	0.9
<i>NONAME</i>	8/3/2007	TD	30	2.3	15.4	26.4	11.0
PABUK	8/7/2007	CAT1	65	49.4	33.4	20.7	-12.7
<i>FITOW</i>	9/4/2007	CAT1	75	43.1	38.6	30.6	-8.0
NARI	9/11/2007	TD	20	14.7	7.7	NaN	NaN
NARI	9/16/2007	CAT1	75	27.0	38.6	48.1	9.5
FRANCISCO	9/22/2007	TD	25	28.8	12.9	33.4	20.5
LINGLING	10/14/2007	TS	35	21.3	15.4	46.4	31.0
<i>KAJIKI</i>	10/21/2007	CAT4	115	10.9	48.9	48.4	-0.5
<i>PEIPAH</i>	11/4/2007	CAT1	65	37.4	33.4	36.3	2.9
MITAG	11/24/2007	CAT2	85	31.2	43.7	32.2	-11.5
NONAME	11/26/2007	TD	25	17.9	12.9	NaN	NaN
<i>NAKRI</i>	5/31/2008	CAT2	95	39.0	36.0	34.0	-2.0
<i>NAKRI</i>	6/2/2008	CAT2	85	21.3	38.6	25.4	-13.2
KALMAEGI	7/12/2008	TD	20	37.8	10.3	23.0	12.7
KALMAEGI	7/19/2008	TD	30	28.1	15.4	30.3	14.9
FUNG-WONG	7/25/2008	TS	35	18.2	18.0	29.0	11.0
FUNG-WONG	7/29/2008	TD	20	18.8	12.9	21.3	8.4
KAMMURI	8/5/2008	TS	45	22.7	23.1	25.5	2.4
NURI	8/16/2008	TS	50	32.5	7.7	36.0	28.3
SINLAKU	9/7/2008	TD	20	29.0	12.9	19.5	6.6

HAGUPIT	9/21/2008	CAT1	80	46.6	38.6	41.7	3.1
JANGMI	9/25/2008	CAT1	80	19.8	41.2	35.9	-5.3
MEKKHALA	9/29/2008	TS	40	17.0	20.6	32.6	12.0
HIGOS	9/30/2008	TS	40	42.2	23.1	51.3	28.2
MAYSAK	11/6/2008	TD	30	23.5	18.0	38.1	20.1
KUJIRA	5/6/2009	CAT3	100	21.3	51.4	39.5	-11.9
LINFA	6/16/2009	TD	20	33.7	10.3	23.5	13.2
NANGKA	6/25/2009	TS	45	5.3	23.1	19.3	-3.8
GONI	8/3/2009	TD	30	44.0	15.4	NaN	NaN
VAMCO	8/22/2009	CAT3	110	31.9	48.9	32.7	-16.3
KROVANH	8/31/2009	TS	55	16.2	23.1	32.2	9.1
CHOI-WAN	9/15/2009	CAT4	130	23.3	66.9	49.8	-17.1
KETSANA	9/27/2009	TS	55	4.5	28.3	52.3	24.0
EIGHTEEN	9/28/2009	TD	30	26.0	15.4	33.3	17.9
EIGHTEEN	9/28/2009	TD	30	7.6	10.3	44.5	34.2
PARMA	9/30/2009	CAT3	105	38.4	51.4	37.4	-14.0
MELOR	10/8/2009	TS	45	16.1	25.7	12.7	-13.0
MELOR	10/9/2009	TS	45	13.0	23.1	NaN	NaN
LUPIT	10/16/2009	CAT1	80	30.6	33.4	38.4	5.0
LUPIT	10/21/2009	CAT1	75	22.1	41.2	46.8	5.6
MIRINAE	10/31/2009	TS	55	47.7	28.3	38.0	9.7
TWENTYFIVE	11/8/2009	TS	45	48.5	23.1	NaN	NaN
TWENTYSEVEN	11/22/2009	TD	20	33.3	12.9	25.2	12.3
NIDA	11/28/2009	CAT4	125	17.3	66.9	36.3	-30.7
NIDA	11/30/2009	CAT3	100	8.3	51.4	44.8	-6.6
SANVU	5/27/2012	TS	50	46.1	25.7	NaN	NaN
JELAWAT	9/29/2012	CAT3	100	43.0	51.4	32.7	-18.7
GAEMI	10/5/2012	TS	35	13.6	18.0	45.1	27.1
MARIA	10/19/2012	TD	30	25.1	15.4	14.6	-0.8

C. RESULTS BY CATEGORY

1. Saffir-Simpson Scale of Intensity

A summary of the estimated accuracy (Table 11) is defined in Tables 12 and 13 stratified by storm intensity scale, and separated with all TC cases above and only those 22 cases with a clear center below.

Table 12. Average intensity difference (m s^{-1}) by Saffir-Simpson scale for all 65 cases.

Type	[Vmax – BT] Average	Count
TD	16.5	19
TS	10.4	17
CAT 1	-1.3	14
CAT 2	-10.8	4
CAT 3	-14.8	6
CAT 4	-15.2	4
CAT 5	-42.6	1

Table 13. Average intensity difference (m s^{-1}) by Saffir-Simpson scale for the 22 clear center cases.

Type	[Vmax – BT] Average	Count
TD	5.1	3
TS	5.3	1
CAT 1	-0.6	6
CAT 2	-7.6	2
CAT 3	-15.4	5
CAT 4	-15.2	4
CAT 5	-42.6	1

Similar to the results from Luo et al. (2008), over the entire dataset there is an over estimation of weak storms and an under estimation of strong storms. The results with respect to storm intensity are also evident in the cases with a clear center, but with a reduction in the error magnitude. The error in maximum wind estimate for weak storms in the early life cycle of TC development may be due to concentrated areas of convective towers. These convective towers can cause the over estimation of the storm intensity due to an accented slope in cloud-top height, which would impact Δh^* . However, when the life cycle has evolved to a stage were a center of circulation is established the method has the ability to more accurately estimate storm intensity. This will be investigated in the following section that examines individual cases. The individual cases of estimated versus actual intensity is categorized by the Saffir-Simpson scale in Figure 8. The image

on the left represents all storms in the dataset while the image on the right contains the cases where a clear center is identified. The black dashed line is a reference line of equal estimated and actual intensities. The red oval is placed to showcase the under-estimated weak TCs that are removed when only the TCs with a clear center are considered.

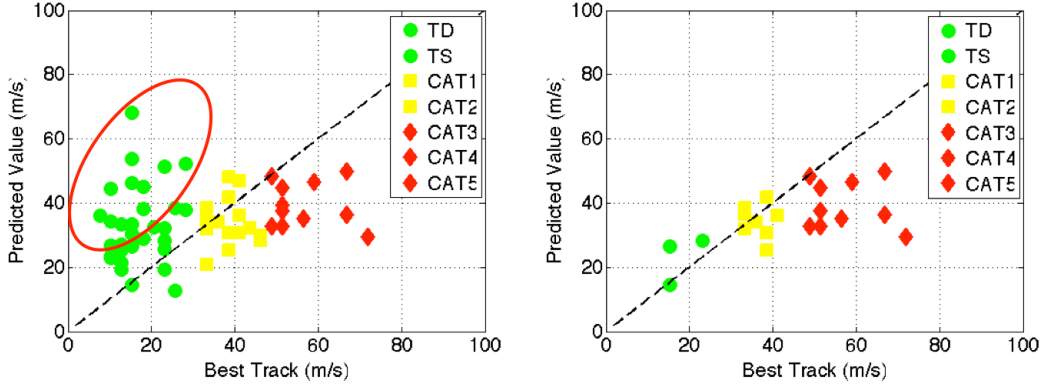


Figure 8. Estimated versus best track tropical cyclone maximum wind speed (m s^{-1}) categorized by the Saffir-Simpson intensity scale for all TCs on the left and TCs with a clear center on the right.

The statistical significance of the maximum wind estimates in cases of a clear center is examined in Table 14 by the Saffir-Simpson intensity scale. Significance is determined with a t-test that accounts for sample size. The significance of the estimation technique is dominated by the accuracy in estimating maximum wind speeds for storms of less than category 2 intensity where a clear storm center is evident. However, the maximum wind of intense storms are under estimated.

Table 14. Linear correlation between the estimated and actual maximum wind speeds for the TC cases with a clear center. Correlations that are statistically significant at a 95% level are in bold.

Intensity	R	R^2
TD & TS	0.61	0.37
CAT1 & CAT2	-0.13	0.017
CAT3 – CAT5	-0.11	0.012
TD – CAT2	0.69	0.48
All	0.57	0.32

2. Overpass Distance to TC center

The importance of the overpass distance to the storm center, which is the fifth column titled “Min Dist” in Table 12 is defined in Figure 9. The overpass distance is defined by terciles at 18 and 31 km. The image on the left represents all storms in the dataset while the image on the right represents the cases where a clear center is identified. The green markers represent overpasses close to the storm center, while red markers indicate overpasses at a relative far distance. Again, there is an improvement in the accuracy when only those TCs with a clear center are considered. It is clear for Figure 9, that the under estimate of the maximum winds for the most intense storms is reduced when the distance between the storm center and overpass is small.

The increase in accuracy with decreasing overpass distance was expected due to the method utilized to calculate the total moist static energy difference, Δh^* . The method used the cloud-top height closest to the storm center and averaged the slope outward in both directions from the storm center. In cases where the overpass distance was in the upper third, this meant that the calculation would often be performed using a measurement of cloud-top height that did not represent the TC center. This would cause the resultant estimated maximum sustained wind to also be inaccurate.

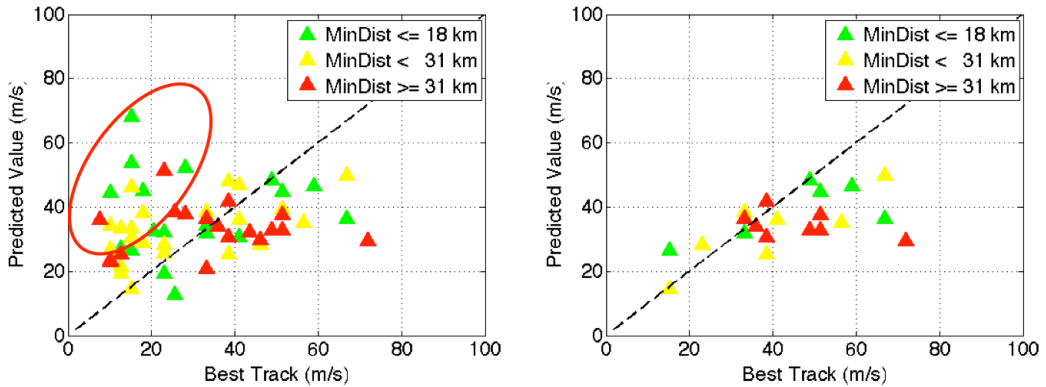


Figure 9. Estimated versus best track tropical cyclone maximum wind speed (m s^{-1}) categorized by the satellite overpass distance to the storm center (in km). All TCs are on the left and only TCs with a clear center are on the right.

The estimate of maximum wind speed from the clear center TCs is examined for statistical significance in Table 15 by the overpass distance to the storm center. The categories possessing a statistical significance are highlighted in bold-italic font. The first category of less than 18 km does not contain enough cases to be significant. However, the middle distance, and combination of all distances are statistically significant.

Table 15. As in Table 13, except for distance between the satellite overpass and the storm center.

Overpass Distance (km)	R	R ²
TCs \leq 18	0.69	0.48
<i>18 \leq TCs \leq 31</i>	<i>0.83</i>	<i>0.69</i>
TCs \geq 31	-0.49	0.25
<i>TCs \leq 31</i>	<i>0.77</i>	<i>0.60</i>
<i>All</i>	<i>0.57</i>	<i>0.32</i>

3. Change in Total Moist Static Energy

As defined in Chapter III, the change in the total moist static energy, Δh^* , can be considered as the slope of the cloud-top height from the inner to outer core. Here, it was defined from the CTH at the center of the TC averaging outward in either direction to an estimation where zero dBZ was observed by the cloud profiling radar. The relationship between Δh^* and maximum wind is characterized in Figure 10 with the plot on the left representing all TCs within the dataset and the plot on the right representing those TCs with a clear center. The markers separate the data into thirds with the green markers indicating storms with a shallow slope, while the red markers indicate storms with a steep slope. A high value or very steep slope as a measure of change in total moist static energy often represents a TC that is intensifying. Once the TCs without a clear center are removed a significant number of the red markers at weak intensities are removed. As eluded to above and will be shown in Chapter V, weak TCs often contain isolated bursts of deep convection before a well-defined center appears. A satellite overpass in a region of isolated convection measures a steep slope and thus a high Δh^* . However, this

measure is not representative of the overall circulation. Additionally, it is clear that the most under estimated maximum wind values are characterized by small values of Δh^* .

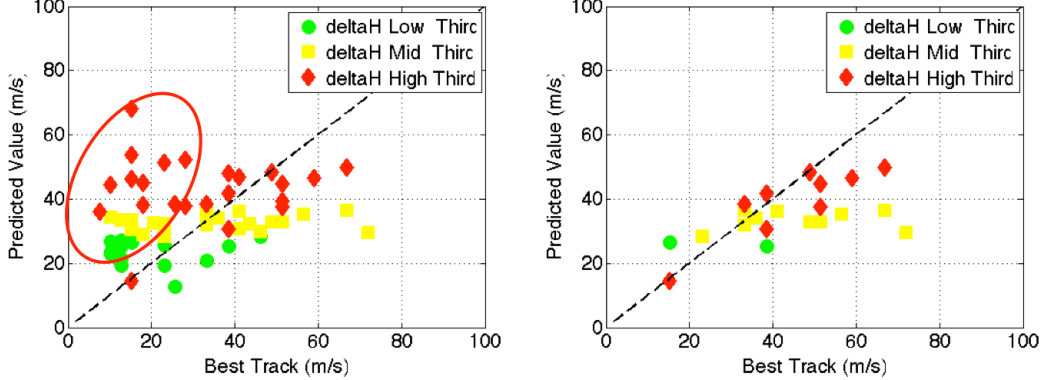


Figure 10. Estimated versus best track tropical cyclone maximum wind speed ($m s^{-1}$) categorized by the change in total moist static energy from the inner to outer core. All TCs are on the left and only TCs with a clear center are on the right.

4. Shear

The method of TC intensity estimation defined by (5) is most effective when the storm is symmetric. Since shear can cause asymmetry in TC structure, the amount of vertical shear over a TC was another factor analyzed for its impact to the estimated maximum sustained wind. This relationship is characterized in Figure 11 with the plot on the left representing all TCs within the dataset and the plot on the right representing those TCs with a clear center. The markers separate the data into thirds with the green markers indicating storms with a relatively low amount of shear, while the red markers indicate storms with a relatively high amount of shear. Once again the storms inside the red oval are removed, when only TCs with a clear center are identified. The relationship to vertical wind shear is not defined clearly. The removed storms are distributed through all categories of shear without a clear correlation to the amount of shear and the estimated TC intensity.

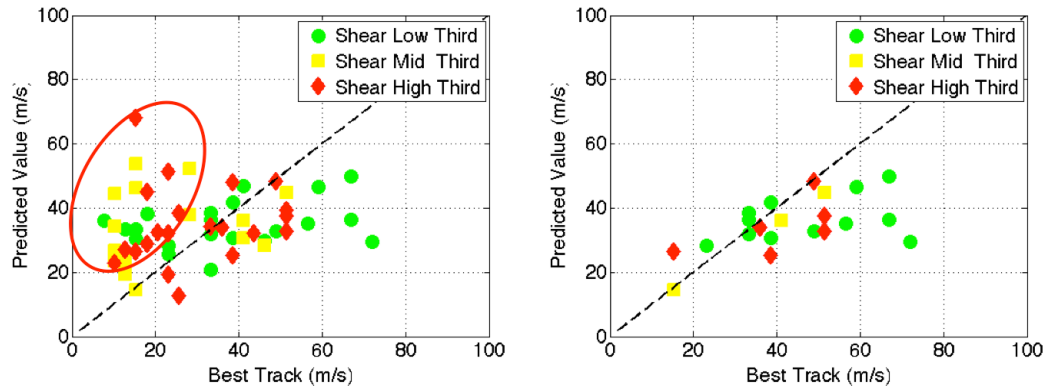


Figure 11. Estimated versus best track tropical cyclone intensity categorized by storm shear.

V. CASE STUDIES

In general, the use of (5) for estimating TC maximum wind using data from CloudSat has overestimated weak TCs and underestimated intense TCs. In this chapter, examples are provided for cases in which this method provided accurate maximum wind estimates, overestimates of a weak TC, and underestimates of an intense TC.

A. WEAK CORRELATION

1. TD BILLIS – 8 July 2006

The overpass of TD BILLIS occurred from 1631 – 1634 UTC on 8 July 2006. This case is a clear example of the overestimation of maximum winds in a weak TC. In this case the difference between estimated maximum sustained wind and the actual wind is 38.5 m s^{-1} (Table 11). At this time, the TC does not have a clearly defined center of circulation. The satellite overpass is directly over the deep convective tower identified in the AMSR-E imagery (Figure 12a) as the red circular area in the center of the pass. This deep convection is evident in the CloudSat reflectivity image of Figure 12e, causing an over-estimation of the total moist static energy and the overall estimated intensity. Based on the measured cloud-top height, a large slope existed for the center of the convective cluster to the environment, which resulted in a large parameterized Δh^* . This case of a weak TC without a central circulation is a typical example of an overestimate of a weak TC.

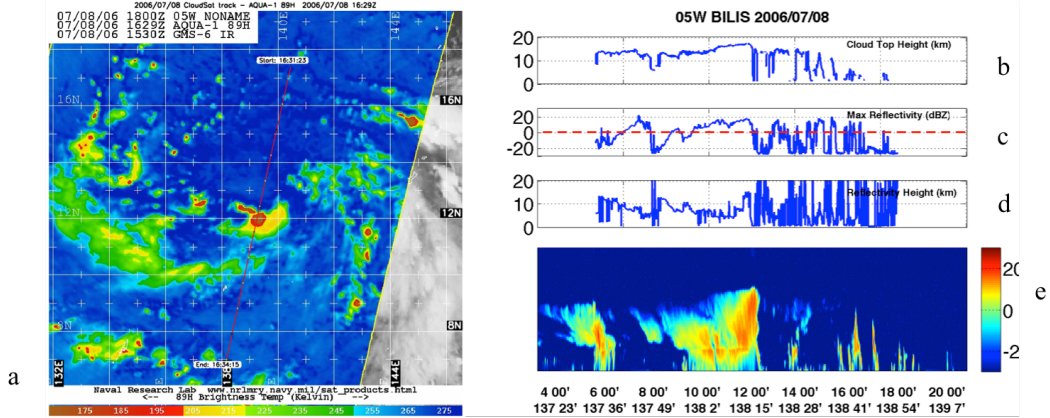


Figure 12. (a) The 89 GHz Aqua microwave and MTSAT infrared image composite of TD Billis at 1530 UTC 8 July 2006, (b) CloudSat derived cloud-top height (km), (c) maximum reflectivity (dBZ), (d) height of maximum reflectivity (km), (e) reflectivity cross-section (dBZ)

2. Category 4 CHOI-WAN—15 September 2009

The CloudSat overpass of Typhoon CHOI-WAN occurred from 0334-0352 UTC 15 September 2009. At the time, TY Choi-Wan was a very strong category four typhoon with winds of 130 kt (67 m s^{-1}). The AQUA satellite infrared imagery (Figure 13a) and CloudSat reflectivity (Figure 13e) identify the classic example of a mature TC structure. Although, the satellite overpass was within 23 km of the eye and the cloud-top height (Figure 13b) exhibit a pronounced slope, the method underestimated the storm intensity by 17 m s^{-1} (Table 11). The error can best be attributed to the assumptions made by approximating Eq. (5) from Eq. (4) in that the neglect of the surface pressure difference term in the denominator of Eq. (5) may prevent increased estimates of maximum wind speed.

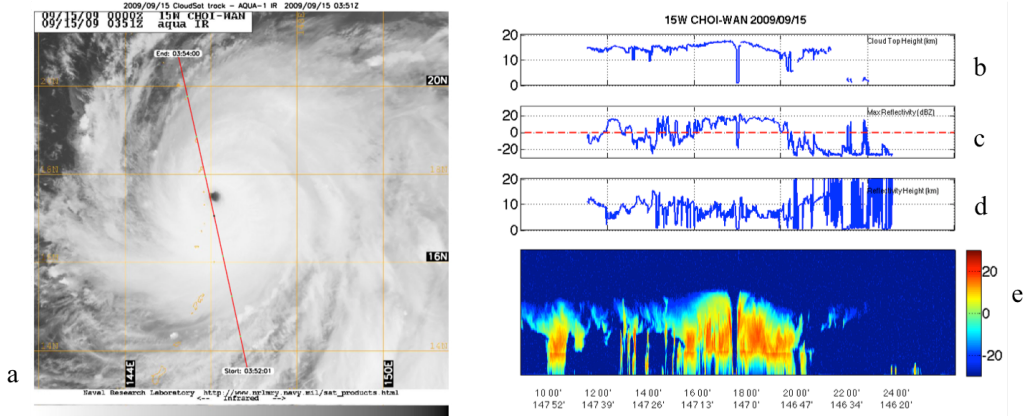


Figure 13. (a) Infrared image from Aqua at 0351 UTC 15 September 2009 of category four Choi-Wan, (b) Cloud-top height (km), (c) maximum reflectivity (dBZ), (d) height of maximum reflectivity (km), and (e) reflectivity cross-section (dBZ)

3. Category 5 YAGI—21 September 2006

The time of overpass of Typhoon Yagi occurred from 1603-1611 UTC 21 September 2006. TY Yagi was a very strong category five typhoon with winds of 140 kt (72 m s^{-1}). This storm was the only category five typhoon with valid overpass data for this study. The satellite overpass occurs at 40 km from the storm center, which is near the outer limit for the WE2007 method. As a result, the use of Eq. (5) results in a significant underestimation of the TC intensity. This overpass occurs over a region just outside the eyewall (Figure 14a) where there is relatively little changes in the slope of the cloud-top height (Figure 14b-e). This leads to an underestimation of the change in moist static energy and the estimated maximum sustained winds that are 29 m s^{-1} too low (Table 11).

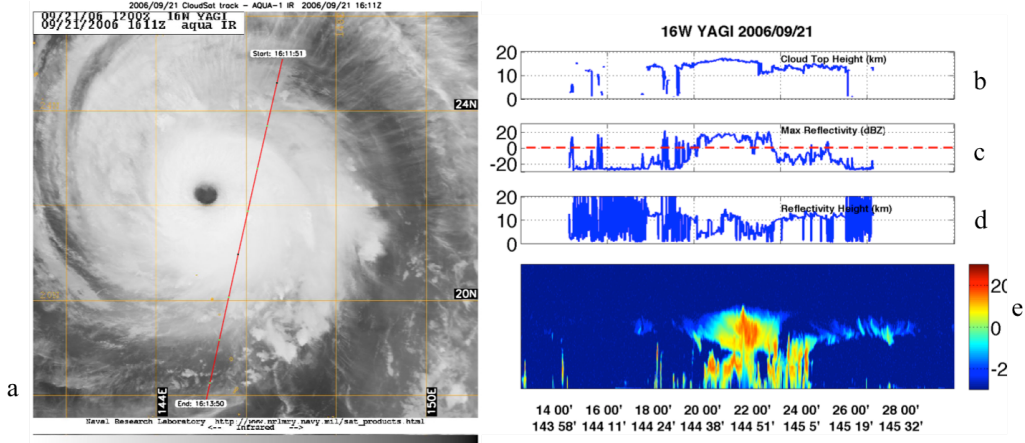


Figure 14. (a) Infrared image from Aqua at 1611 UTC 21 September 2006 of category five Yagi, (b) Cloud-top height (km), (c) maximum reflectivity (dBZ), (d) height of maximum reflectivity (km), and (e) reflectivity cross-section (dBZ)

B. STRONG CORRELATION

1. Category 1 PRAPIROON—02 August 2006

The time of overpass of Typhoon Papiroon occurred from 0552-0554 UTC 02 August 2006. TY Papiroon was a developing category one typhoon with winds of 65 kt (33 m s^{-1}). In Figure 15a, there is a clear center of circulation identifiable in the AQUA infrared image. The center is also seen in the CloudSat reflectivity (Figure 15e). The satellite overpass distance of 3 km provides an accurate representation of the variation in cloud-top height across the storm center. Therefore the estimate of maximum sustained winds was only 1 m s^{-1} too low.

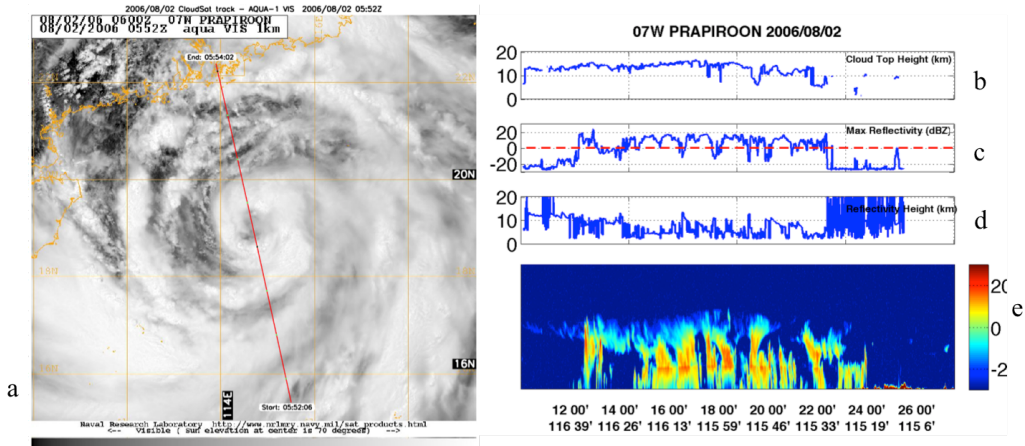


Figure 15. (a) Infrared image from Aqua at 0552 UTC 02 August 2006 of category one Prapiroon, (b) Cloud-top height (km), (c) maximum reflectivity (dBZ), (d) height of maximum reflectivity (km), and (e) reflectivity cross-section (dBZ)

2. Category 3 NIDA—30 November 2009

The time of overpass of Typhoon Nida occurred from 0416-0419 UTC 30 November 2009. TY Nida was a mature category three typhoon with winds of 100 kt (51 m s⁻¹). The display in Figure 16 exhibits the model structure in infrared and CloudSat reflectivity images with a clearly identifiable center of circulation. The satellite overpass occurs within 8 km of the storm center (Figure 16a) and a clear center is identifiable at the time of the pass. The overpass over the clearly defined center provides a well-defined measure of cloud-top height (Figure 16b) and reflectivity (Figure 16c,e). As a result, the estimate maximum winds are only 6 m s⁻¹ too low.

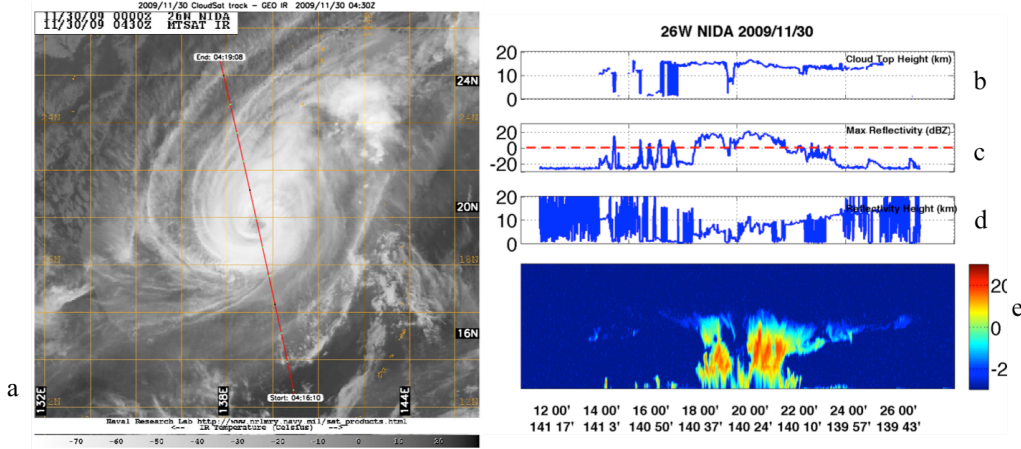


Figure 16. (a) Infrared image from MTSAT at 0430 UTC 30 November 2009 of category four Nida, (b) Cloud-top height (km), (c) maximum reflectivity (dBZ), (d) height of maximum reflectivity (km), and (e) reflectivity cross-section (dBZ)

3. Category 4 KAJIKI—21 October 2007

The time of overpass of Typhoon Kajiki occurred from 0344-0347 UTC 21 October 2007. TY Kajiki was a very strong category four typhoon with winds of 115 kt (49 m s^{-1}) and had intensified 10 kt over the last 12 hours. The satellite overpass occurs a distance of 11 km, which is in lowest third of overpass values. The AMSR-E satellite and CloudSat reflectivity images in Figure 17a,e identify a clear center of circulation and TC structure. Again, the proximity of the overpass and the clearly defined center lead to an estimate error of only -1 m s^{-1} .

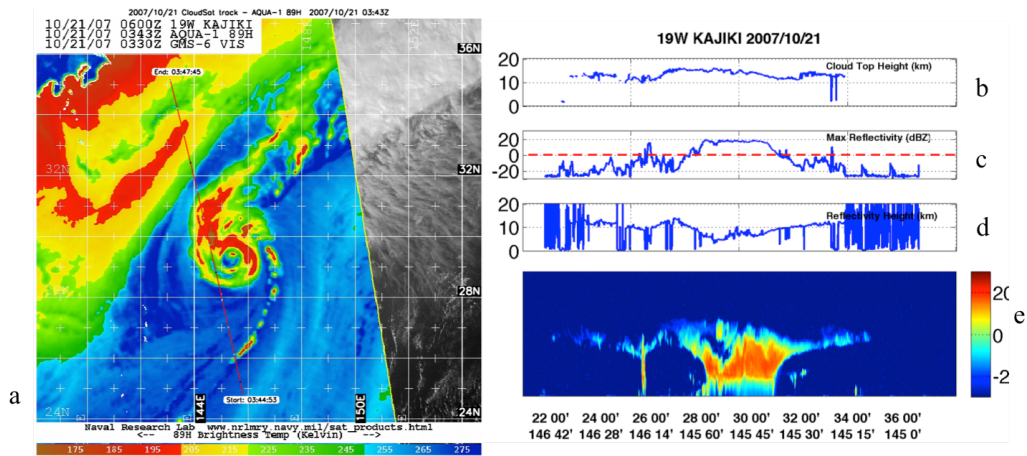


Figure 17. (a) A 89 GHz Aqua microwave and GMS-6 visible image composite of category five Kajiki at 0330 UTC 21 October 2007, (b) CloudSat derived cloud-top height (km), (c) maximum reflectivity (dBZ), (d) height of maximum reflectivity (km), (e) reflectivity cross-section (dBZ)

THIS PAGE INTENTIONALLY LEFT BLANK

VI. CONCLUSIONS

A. UTILITY OF CPR MEASUREMENTS AND THE A-TRAIN

CloudSat and the A-Train constellation have provided the first statistics on the vertical structure of clouds from space. This thesis demonstrates that there is utility in applying these statistics measured by CloudSat and other members of the A-Train constellation to estimating TC intensity by way of the maximum sustained wind. This is possible by employing Eq. (4) developed by Wong and Emanuel (2007) that was then approximated by Luo et al. (2008) to neglect the representation of the earth angular momentum and a factor related to the surface pressure deficit.

This thesis expanded the data set and methodology employed by Luo et al. (2008) of estimating the maximum sustained winds using satellite based cloud-top slope estimates. The data set included 65 cases after removing overpasses, which did not have best track or cloud top temperature data. For calculation of cloud-top slope the outer location is defined by calculating the difference in cloud-top height from the highest clouds near the TC center to the related location where reflectivity first becomes zero dBZ. The measure of h^* was defined from the cloud-top height on each side of the center of the TC, or the closest point of approach between the satellite overpass and the storm center. These values were then averaged before input into Eq. (5) as Δh^* , which produced an estimated value for the maximum sustained wind. Due to the importance of the TC center, the data were further stratified to 22 cases characterized by having a clear center circulation.

A primary objective of this thesis was to examine sensitivities of estimate maximum wind to the overpass distance to the TC center, the TC intensity, and TC structure asymmetries due to vertical wind shear. A significant dependency was identified to the distance between the satellite overpass and TC center. A strong significant sensitivity was also found to TC intensity. In general, for all cases there was an over-estimation of weaker storms and an under estimation of strong storms. The under estimate of mature TCs was often due to a smooth slope when the satellite overpass

did not achieve an eye or near-eye overpass, and the overestimate of weaker TCs was often due to the steeper slope associated with the deep convective towers observed in developing storms. The greatest accuracy is found where the satellite overpass was relatively near the TC center, which allowed for measurements of cloud-top slope that represented Δh^* .

The most accurate results were observed when the dataset was reduced to those TCs exhibiting a clear center of circulation. This is due to the change in total moist static, Δh^* , energy calculated utilizing the cloud-top height from the center of the TC averaged outward in both directions through the slice of the TC. When considering only the TC with a clearly identifiable center, the accuracy is improved by an average of 5 m s^{-1} ¹ for storms of intensity ranging from TD through category two.

There was some sensitivity identified related to the shear over a given TC, which impacts TC structure as well as the representation of the change in the total moist static energy defined by cloud-top slope. However, the observed sensitivity to shear was not varying over TC intensity as the general estimated maximum wind varies. In conclusion, the CloudSat and A-Train data provide a valuable resource for estimate of maximum wind speeds in TCs over data sparse regions. However, the estimations exhibit strong sensitivities to the satellite overpass proximity to the TC center. The method used to estimate change in moist static energy from measurements of cloud properties from space contains well-defined biases that overestimate winds in weak TCs and underestimates winds in intense TCs.

B. RECOMMENDATIONS

Emerging technology such as the CPR onboard the satellite CloudSat and the A-Train constellation have provided the opportunity for additional information on TC structure, intensity, and vertical distribution of rainfall. The case studies highlight examples of when the method has strong and weak correlation between the estimated maximum sustained wind and the best track data obtained from the JTWC archive. The sun synchronous orbit of the A-Train constellation does not allow it to replace techniques such as the Dvorak method for TC intensity estimation in areas lacking *in situ*

measurements. However, using these examples and the aforementioned sensitivities as a guideline, this method has the potential to be another tool to aid forecasters in accurate prediction of TC intensity in regions where *in situ* data is scarce.

THIS PAGE INTENTIONALLY LEFT BLANK

LIST OF REFERENCES

Brennan, J., H. J. Lee, M. Yang, M. Folk, and E. Pourmal, 2013: Working with NASA's HDF and HDF-EOS earth science data formats. *The Earth Observer*, **25**, 2, 16–20.

Central Pacific Hurricane Center, cited 2012: Our Mission. [Available online at <http://www.prh.noaa.gov/cphc/pages/mission.php>.]

Colorado State University, cited 2014: 2006-2013 CloudSat tropical cyclone HDF files and images. [Available online at <http://reef.atmos.colostate.edu/~natalie/tc/>].

CloudSat Mission, cited 2014: CloudSat. [Available online at <http://cloudsat.atmos.colostate.edu/>].

Cooperative Institute for Research in the Atmosphere (CIRA), 2008. *CloudSat Standard Data Products Handbook*. Colorado State University, 18 pp.

Dorsey, J., 2003: Navy costs for Isabel at least \$105.6 million. 27 September, *Virginian-Pilot*, A18.

Durden, S. L., S. Tanelli, and G. Dobrowalski, 2009: CloudSat and A-Train observations of tropical cyclones. *The Open Atmospheric Science Journal*, **3**, 80–92, doi:10.2174/1874282300903010080.

Emanuel, K. A., 1986: An Air-Sea Interaction Theory for tropical cyclones. Part I: steady-state maintenance. *J. Atmos. Sci.*, **43**, 585–605.

Emanuel, K., 2005: Nature's Steam Engine. *Divine Wind: The History and Science of Hurricanes*. Oxford University Press, 54-61.

Im, E., S. L. Durden, Chialin Wu, and T. R. Livermore, 2001: The 94-GHz cloud profiling radar for the CloudSat mission. *Proc. Aerospace Conference, 2001, IEEE Proceedings*, **4**, 4/1803-4/1809.

Joint Typhoon Warning Center, cited 2012: Mission Statement. [Available online at <http://www.usno.navy.mil/JTWC/>].

NASA, Jet Propulsion Laboratory, n.d.: NASA facts, CloudSat fact sheet. [Available online at http://www.nasa.gov/pdf/136796main_cloudsat-factsheet.pdf.]

Luo, Z., G. Y. Liu, and G. L. Stephens, 2008: CloudSat adding new insight into tropical penetrating convection. *Geophys. Res. Lett.*, **35**, L19819, doi:10.1029/2008GL035330.

Luo, Z., G. L. Stephens, K. A. Emanuel, D. G. Vane, N. D. Tourville, and J. M. Haynes, 2008: On the use of CloudSat and MODIS data for estimating hurricane intensity. *IEEE Geoscience and Remote Sensing Letters*, **5**, 13–16, doi:10.1109/LGRS.2007.905341.

Mitrescu, C., S. Miller, J. Hawkins, T. L'Ecuyer, J. Turk, P. Partain, and G. Stephens, 2008: Near-Real-Time applications of CloudSat data. *J.Appl.Meteor.Climatol.*, **47**, 1982–1994, doi:10.1175/2007JAMC1794.1.

National Hurricane Center, 2013: About the National Hurricane Center. [Available online at <http://www.nhc.noaa.gov/aboutintro.shtml>.].

Nayak, M., M. Witkowski, D. Vane, T. Livermore, M. Rokey, M. Barthuli, I. Gravseth, B. Pieper, A. Rodzinak, S. Silva, and P. Woznick, 2012: CloudSat anomaly recovery and operational lessons learned. *Proc. SpaceOps 2012*, Stockholm, Sweden, 1-14.

Stephens, G. L., D. G. Vane, R. J. Boain, G. G. Mace, K. Sassen, Z. Wang, A. J. Illingworth, E. J. O'Connor, W. B. Rossow, S. L. Durden, S. D. Miller, R. T. Austin, A. Benedetti, C. Mitrescu, and S. T. CloudSat, 2002: The CloudSat mission and the A-Train. *Bull.Amer.Meteor.Soc.*, **83**, 1771–1790, doi:10.1175/BAMS-83-12-1771.

Velden, C., B. Harper, F. Wells, J. L. Beven, R. Zehr, T. Olander, M. Mayfield, C. Guard, M. Lander, R. Edson, L. Avila, A. Burton, M. Turk, A. Kikuchi, A. Christian, P. Caroff, and P. McCrone, 2006: The Dvorak tropical cyclone intensity estimation technique: A satellite-based method that has endured for over 30 years. *Bull.Amer.Meteor.Soc.*, **87**, 1195–1210, doi:10.1175/BAMS-87-9-1195.

Wong, V., and K. Emanuel, 2007: Use of cloud radars and radiometers for tropical cyclone intensity estimation. *Geophys.Res.Lett.*, **34**, L12811, doi:10.1029/2007GL029960.

INITIAL DISTRIBUTION LIST

1. Defense Technical Information Center
Ft. Belvoir, Virginia
2. Dudley Knox Library
Naval Postgraduate School
Monterey, California